Supplementary Information

Highly regenerative, fast colorimetric response for organo-toxin and oxo-anions in aqueous medium using discrete luminescent Cd(II) complex in heterogeneous manner with theoretical revelation

Dashrathbhai B. Kanzariya,[a] Tuhin S. Khan,[b] Sourav Das,[c] Prem Lama,[b,d,*] Rajib Bandyopadhyay,[a] Tapan K. Pal[a,*]

[a]Department of Chemistry, Pandit Deendayal Energy University, Gandhinagar 382426, Gujarat, India
[b]CSIR-Indian Institute of Petroleum, Haridwar Road, Mohkampur, Dehradun 248005, India
[c]Department of Chemistry, Institute of Infrastructure Technology Research and Management, Ahmedabad-380026, Gujarat, India.
[d]School of Chemical Sciences, Goa University, Taleigao Plateau, Taleigao 403206, Goa, India.

E-mail: tapan.pal@sot.pdpu.ac.in
        prem.lama@iip.res.in

Experimental section

Materials and Methods

All solvents such as ammonium hydroxide solution (25 %), dimethyl sulphoxide (DMSO), ethanol, *N,N'*-dimethylformamide (DMF), dichloromethane (DCM), ethyl acetate, acetonitrile (MeCN), tetrahydrofuran (THF), chloroform and benzene were procured from S. D. Fine chemicals India, and are used in the experiment after proper purification and drying in accordance with standard procedure wherever required. Reagent grade 8-hydroxy quinoline and $Cd(NO_3)_2 \cdot 4H_2O$ were acquired from Sigma-Aldrich. All the nitro analytes, benzene, toluene, nitrobenzene, sodium dodecyl sulphate, sodium lauryl sulphate, hexanoic acid and ammonia were purchased from Avra synthesis, India. Entire fluorescence experiments were performed in aqueous media using 18.2 MΩ-cm type I ultrapure water by ELGA-PURELAB Classic model.

Caution!!!

All nitro compounds are explosive in nature so it should be handled carefully.

Physical measurements

The infrared (IR) spectra in the range 400−4000 cm^{-1} were measured by making a KBr pallet of the sample on a Perkin-Elmer instrument. The Mettler Toledo Star SW 8.10 system was used to calculate the thermogravimetric analysis (TGA) spectra of all the compounds with heating rate of 5 °C/min. The Bruker D8 Advance Series 2 (CuK_α radiation) was used to measure the powder X-ray diffraction pattern (PXRD) of the sample with a scan rate 3°/min at room temperature. Perkin-Elmer Series II (model 2400) was used to determine the elemental composition of compound. ^1H NMR and ^{13}C NMR of the compound was assessed in DMSO-*d6* with internal standard (Me_4Si) by using 500 FT (JEOL ECX, 500 MHz) instrument. Raman spectra was recorded using Renishaw Raman diode laser with 785 nm (Raman Spectrometer, Renishaw plc). EDX (Energy-dispersive X-ray spectroscopy) of complex **1** was performed with the help of OXFORD Tungsten filament. After oxo-anions sensing experiment, the non-existence of the oxo-anions in the recovered **1** were measured by ICP-OES method by using Perkin Elmer (7300 DV). UV-Vis spectra were recorded by using LAMBDA 35 series and all the fluorescence spectra were collected by using Perkin Elmer LS-55. The excited state life time decay was

measured with the help of Jobin Yvon Spectrofluorometer (Model-FLUOROLOG-FL3-11). The surface morphology was collected on FE-SEM (ZEISS) system.

The fluorescence quantum yield of the complex 1 was determined by using the below equation and quinine sulfate (QS) as a standard compound.[1,2]

$$\Phi_1 = \Phi_{QS} \times \frac{(Gradient)_1}{(Gradient)_{QS}} \times \frac{n_1^2}{n_{QS}^2}$$

Where, Φ_{QS} and Φ_1 are the quantum yield of standard (quinine sulfate, Φ_{QS}=0.54 in 0.1 M H_2SO_4) and studied complex 1 respectively. The "n" corresponds to the refractive index of the solution. The gradient is obtained from the slope of the graph between integrated fluorescence luminescent (FL) intensity versus absorbance of the standard and studied complex.

Thermal stability analyses

Thermogravimetric analysis was performed to calculate the thermal stabilities of all the compounds. The TGA of **1** shows the weight loss of ~8.18 % (expected=8.25 %) which is due to the loss of two axial water molecules in the temperature range of 100-180°C and after that the complex is stable up to 430 °C. All the compounds show loss of two water molecules in the above temperature range.

Synthesis and characterization of 1

8-hydroxy quinoline (494 mg; 3.4 mmol) was dissolved in 15 mL of ethanol and transferred to 100 mL round bottom flask (RBF) and subjected to heating at 70 °C for 10 minutes. $Cd(NO_3)_2 \cdot 4H_2O$ (500 mg; 1.62 mmol) was then added and the reaction mixture (RM) was stirred for 2.5 hours at the same temperature. After that approximately 10 mL of ammonia solution (25 %) was added to reaction mixture to maintain the pH≈12 and reaction mixture was further stirred for 10 minutes. The mixture was finally allowed to cool down to room temperature (RT). After one day yellow crystals were developed in the RBF which was filtered, washed with distilled water (3 consecutive wash of 10 mL distilled water) and subsequently by ethanol (10 mL). Yield: 573 mg, (81%), Anal. calcd. for $C_{18}H_{16}N_2O_4Cd$: C, 49.50; H, 3.69; N, 6.41%. Found: C, 49.37;

H, 3.56; N, 6.48%. FT-IR (KBr cm^{-1}): ν(O-H), 3300-3280, ν(C=N), 1615, ν(C-N, C-O) 1279, 1237, ν(Cd-N, Cd-O) 643, 599; FT-Raman (cm-1): ν(C=N), 1576, ν(Cd-O), 500; ^{1}H NMR (400 MHz, DMSO-*d6*, 25 °C, Si(CH$_3$)$_4$): δ (ppm)= 6.58 (s, 2H), 7.1 (s, 2H), 7.27 (s, 2H), 7.49 (s, 2H), 8.27 (s, 2H), 8.65 (s, 2H); ^{13}C NMR (125 MHz, DMSO-*d6*, 25 °C, Si(CH$_3$)$_4$): δ (ppm)= 111.5, 117, 126, 128, 135.5, 137.5, 147.5, 153.5.

X-ray structural studies

The Bruker SMART APEX CCD diffractometer was used to collect the full single crystal data and unit cell measurement of all the complexes under graphite monochromated MoK$_\alpha$ radiation (wavelength = 0.71073 Å) at room temperature. International X-ray Crystallography table is used to get the scattering factors of the entire atoms, linear absorption coefficients and the anomalous dispersion corrections.[3] With the help of SAINT software, the data integration and reduction were performed.[4] In an individual data set of collected reflection, empirical absorption correction method was employed with SADABS.[5] The XPREP was used to determine the space group.[6] To elucidate the final structure of the compound, the direct methods by SHELXTL-97[7] was used and the refinement was done by full-matrix least-squares on F^2 with a SHELXL-2018 program.[8] X-Seed[9] was used as the graphical interface for the SHELX program suite. The hydrogen atoms are linked with the carbon atoms were placed geometrically and using SHELXL default parameter the hydrogen atoms are treated as a riding atoms. The Table S1 indicates all the parameters (unit cell dimension, refinement parameters and collection of data) of **1**. The important bond angles and bond distances are specified in Table S2.

Fluorescence Sensing Experiments

To perform sensing experiment, the finely ground **1** was well dispersed in aqueous medium (1 mg in 20 mL of 18.2 MΩ-cm type I ultrapure water). For all analyte compounds (TNP, 3-NP, *m*-DNB, NB, *p*-NBA, 2-NP, 2,4-DNP, 2,4-DNT, 4-NP, primary stock solution were prepared in DMF (10^{-1} M) followed by dilution of up to one mM solution in aqueous medium. Anion sensing experiment were carried out by using one mM solutions of Na/K-X (X= Cl$^-$, I$^-$, OAc$^-$, HSO$_3^-$, CN$^-$, SO$_4^{2-}$, NO$_2^-$, NO$_3^-$, CO$_3^{2-}$, CrO$_4^{2-}$, Cr$_2$O$_7^{2-}$, HAsO$_4^{2-}$, AsO$_2^-$ and MnO$_4^-$) in aqueous media.

Fluorescence titration procedures

The titration spectra were recorded upon excitation of **1** at 385 nm with 5 nm excitation/emission slit width and screening range of 400-700 nm. The well dispersed aqueous suspension of **1** was transferred to a standard 1 cm path length quartz cuvette. Luminescent experiment was performed by 20 μL incremental addition of analytes (freshly prepared one mM solutions). After recording first emission spectrum of **1**, the successive luminescent spectrum with analyte was recorded. In every titration after the addition of analyte, the cuvette was shaken very nicely to maintain the uniform dispersion.

Recyclable Luminescence Experiments

After the successful sensing experiments of **1** for the detection of TNP, MnO_4^-, $Cr_2O_7^{2-}$ and CrO_4^{2-}, the compound **1** was recovered by simple filtration followed by washing with ultrapure water. The obtained complex was air dried and further used for next sensing cycle.

Density functional theory study

Spin-polarized non-periodic density functional theory (DFT) calculations were carried out using DMol^3 module in Material Studio 8 (Biovia, San Diego, USA) to study the interaction of neutral trinitrophenol and Oxo anions (MnO_4^-, CrO_4^{2-} and $Cr_2O_7^{2-}$) with the Cd-quinolinate complex $[CdQ_2(H_2O)_2]$.[10] The entire calculations were performed by using basis set double numerical plus polarization (DNP) with polarized d− and p− functions for all non-hydrogen and hydrogen atoms, respectively. The Generalized Gradient Approximation (GGA) by Perdew-Wang (PW91)[11] exchange correlation functional was used. In case of geometry optimization, the convergence criteria were set to 0.05 eV/Å, 0.0001 eV and 0.005 Å corresponding to force, energy and displacement, respectively. A similar DFT setup has been used extensively in previous publications[12,13,14] The energies of the highest occupied molecular orbital (HOMO) and lowest unoccupied molecular orbital (LUMO) were obtained by examining the orbital's property tab during the geometry optimization in DMol^3.

Table S1. Crystal data and structure refinement for **1**.

Table S1 Crystal data and structure refinement for 1.	
Identification code	complex
Empirical formula	$C_{18}H_{16}N_2O_4Cd$
Formula weight	436.73
Temperature/K	298(2)
Crystal system	monoclinic
Space group	$P2_1/c$
a/Å	13.6553(14)
b/Å	5.3152(6)
c/Å	11.4050(12)
α/°	90
β/°	108.258(3)
γ/°	90
Volume/Å^3	786.11(15)
Z	2
ρ_{calc}g/cm^3	1.845
μ/mm^{-1}	1.416
F(000)	436.0
Crystal size/mm^3	$0.250 \times 0.160 \times 0.120$
Radiation	MoKα ($\lambda = 0.71073$)
2Θ range for data collection/°	6.284 to 49.992
Index ranges	$-16 \leq h \leq 16, -6 \leq k \leq 6, -13 \leq l \leq 13$
Reflections collected	8851
Independent reflections	1386 [$R_{int} = 0.0635$, $R_{sigma} = 0.0401$]
Data/restraints/parameters	1386/0/120
Goodness-of-fit on F^2	1.086
Final R indexes [I>=2σ (I)]	$R_1 = 0.0261$, $wR_2 = 0.0540$
Final R indexes [all data]	$R_1 = 0.0367$, $wR_2 = 0.0601$
Largest diff. peak/hole / e Å^{-3}	0.73/-0.45

Table S2. The selected bond distance and bond angle around cadmium metal ion in **1**.

Cd O1 2.253(2)	Cd O1 2.253(2)	Cd N1 2.302(3)
Cd N1 2.302(3)	Cd OW1 2.349(3)	Cd OW1 2.349(3)
O1 Cd O1 180.0	O1 Cd N1 105.32(10)	O1 Cd N1 74.68(10)
O1 Cd N1 74.68(10)	O1 Cd N1 105.32(10)	N1 Cd N1 180.0

O1 Cd OW1 89.96(9)   O1 Cd OW1 90.04(9)   N1 Cd OW1 92.82(10)

N1 Cd OW1 87.18(10)   O1 Cd OW1 90.04(9)   O1 Cd OW1 89.96(9)

N1 Cd OW1 87.18(10)   N1 Cd OW1 92.82(10)   OW1 Cd OW1 180.0
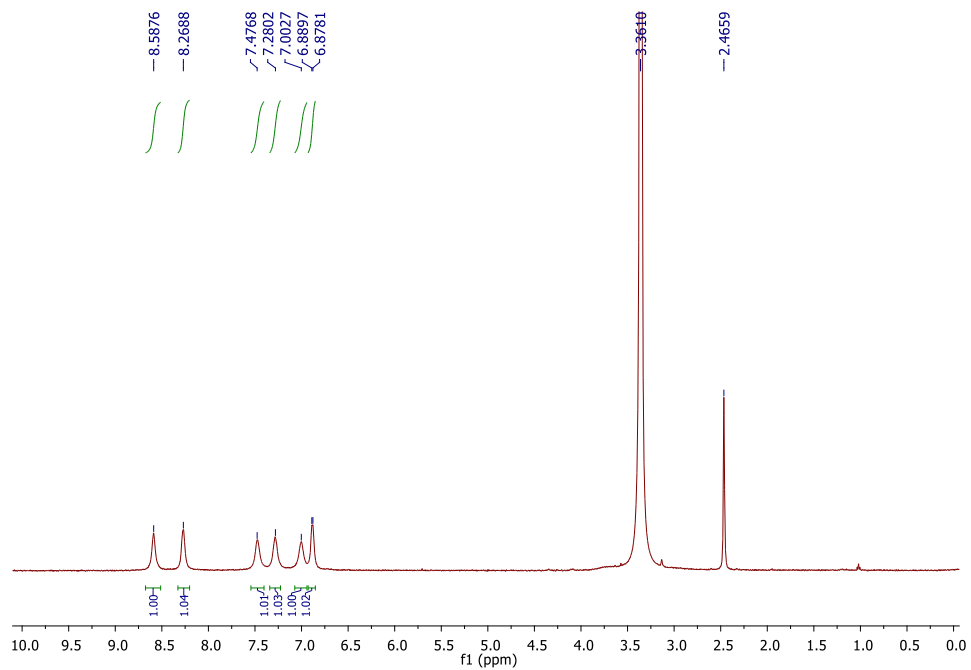
Fig. S1. The ¹H NMR spectrum of **1** in *d₆*-DMSO.
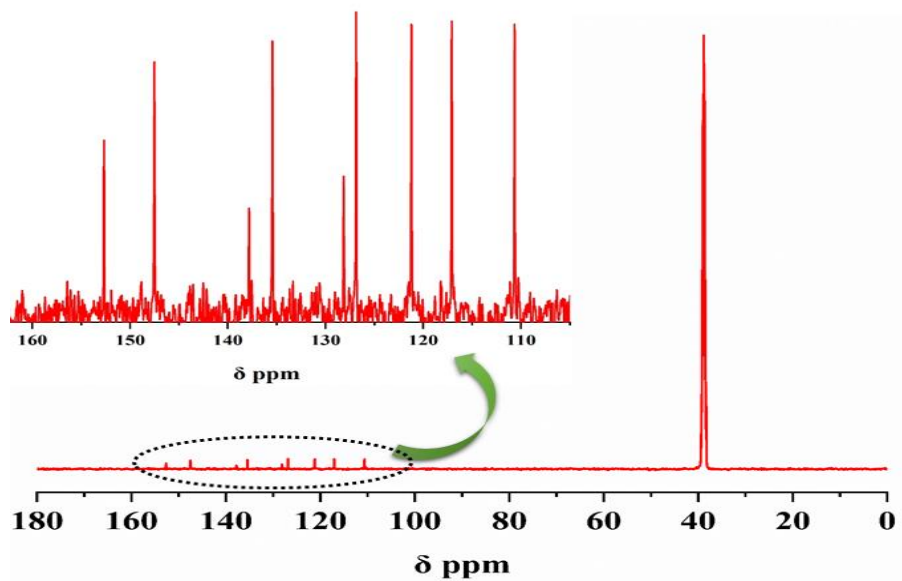
Fig. S2. The ^{13}C NMR spectrum of **1** in d_6-DMSO.
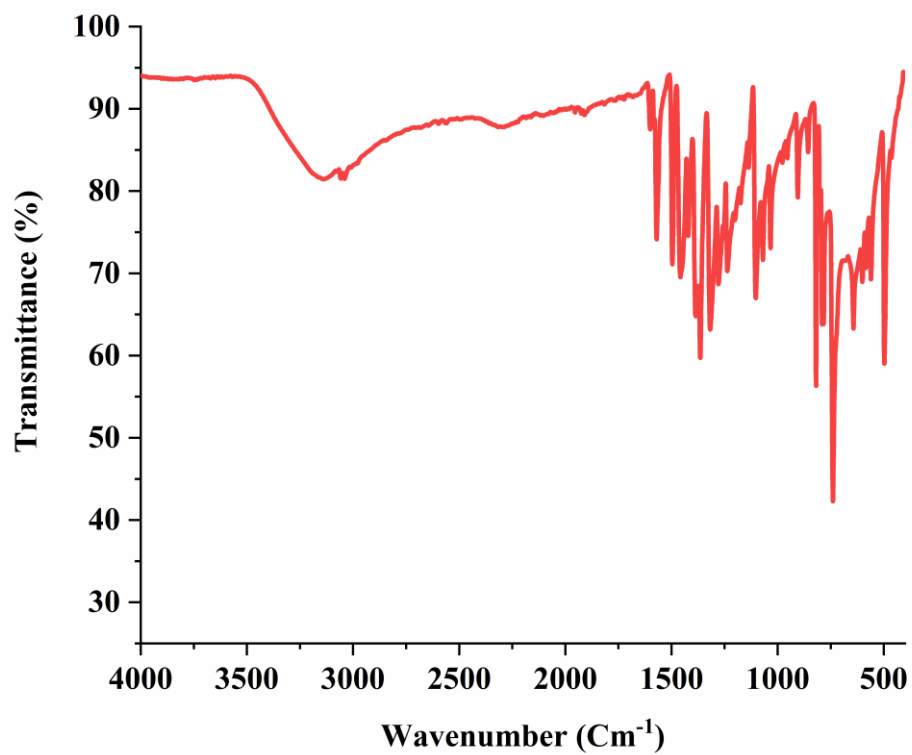
Fig. S3. The FT-IR spectrum of **1.**
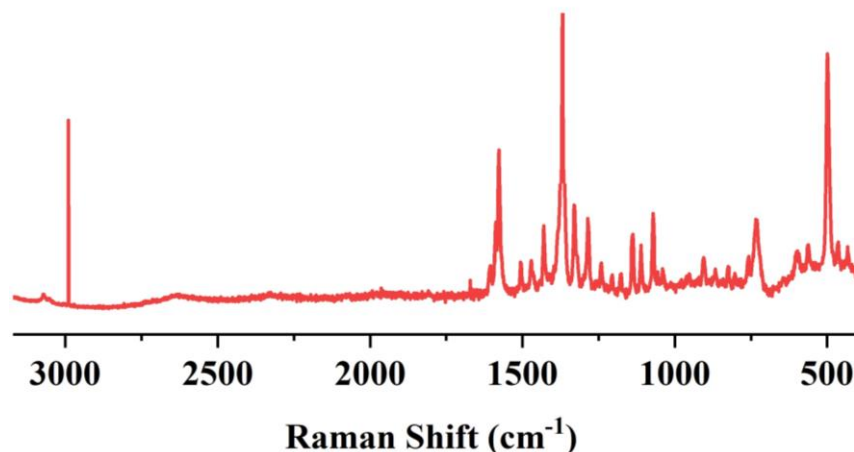
Fig. S4. The Raman spectrum of **1**. The obtained Raman shift (cm^{-1}) for the complex **1** are: ring stretching for v(C=N) 1576, ring stretching frequency v(C-H) 1428 & 1370, while v(C-O) observed at 1070, v(C-N) observed at 732 and v(Cd-O) & v(C-C) 500.

Table S3. IR analysis of **1**.

Wavenumbers (cm^{-1})	Assignment	Wavenumbers (cm^{-1})	Assignment
3300-3280	O-H stretching frequency (broadening due to hydrogen bonding)	1388, 1365 &1318	C-N/C-C stretching and bending of quinoline
3058 & 3040	Stretching frequency of C-H bond of quinoline ring	1279, 1237 & 1104	C-O/C-N stretching, C-H/C-C bending vibrations
1600 & 1570	C-C Stretching vibrations of quinoline ring group	819, 800, 791, 783 & 739	C-H out of plane wagging
1496 & 1459	C-H bending and C-N/C-C stretching vibrations of phenyl and pyridyl group	643, 599, 557 & 495	Cd-N/Cd-O stretching vibrations /Cd–O bending vibrations, CCC bending
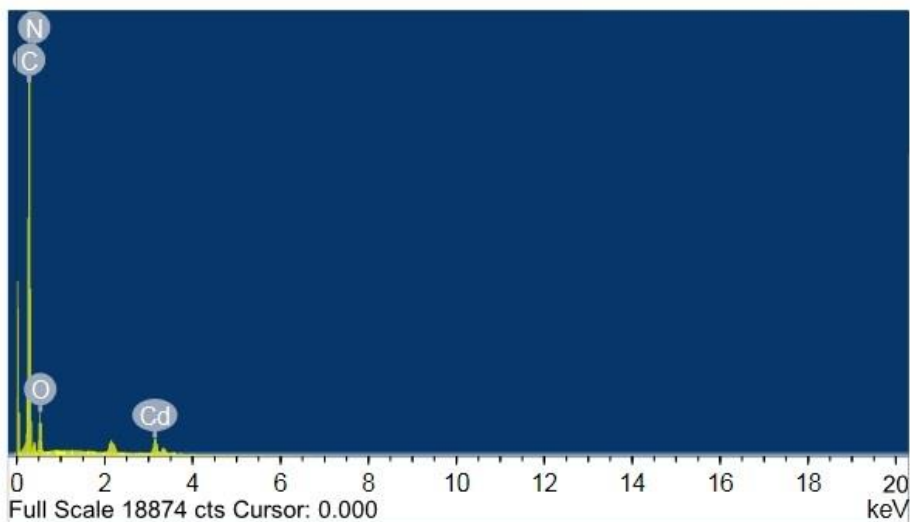
Fig. S5. The EDX spectrum of **1**.
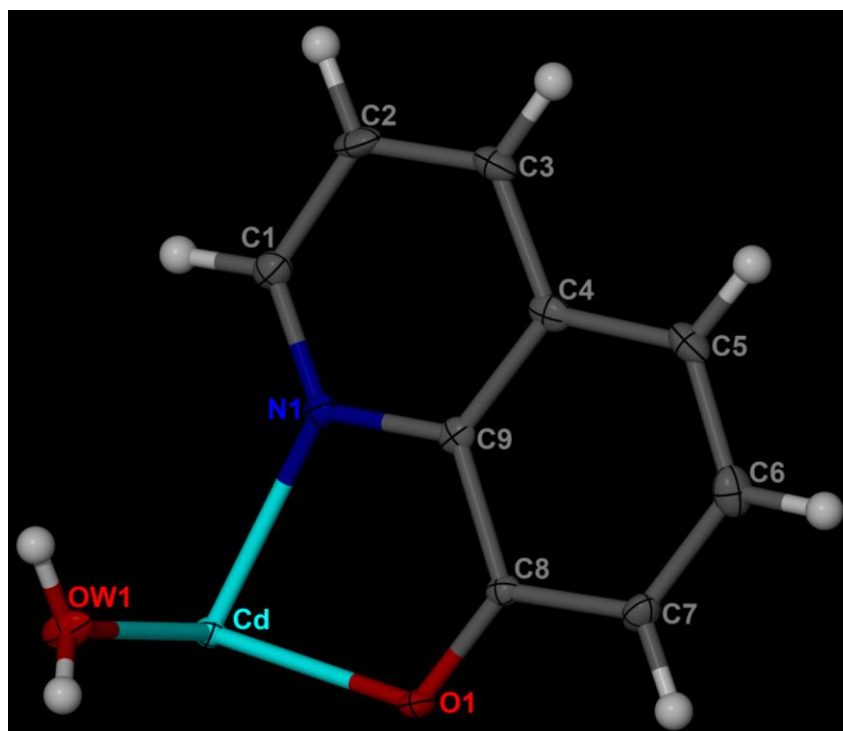
Fig. S6. The asymmetric unit of **1** with 50% ellipsoid probability. The color code: cyan, blue, grey and white are indicating cadmium, nitrogen, carbon and hydrogen element respectively.
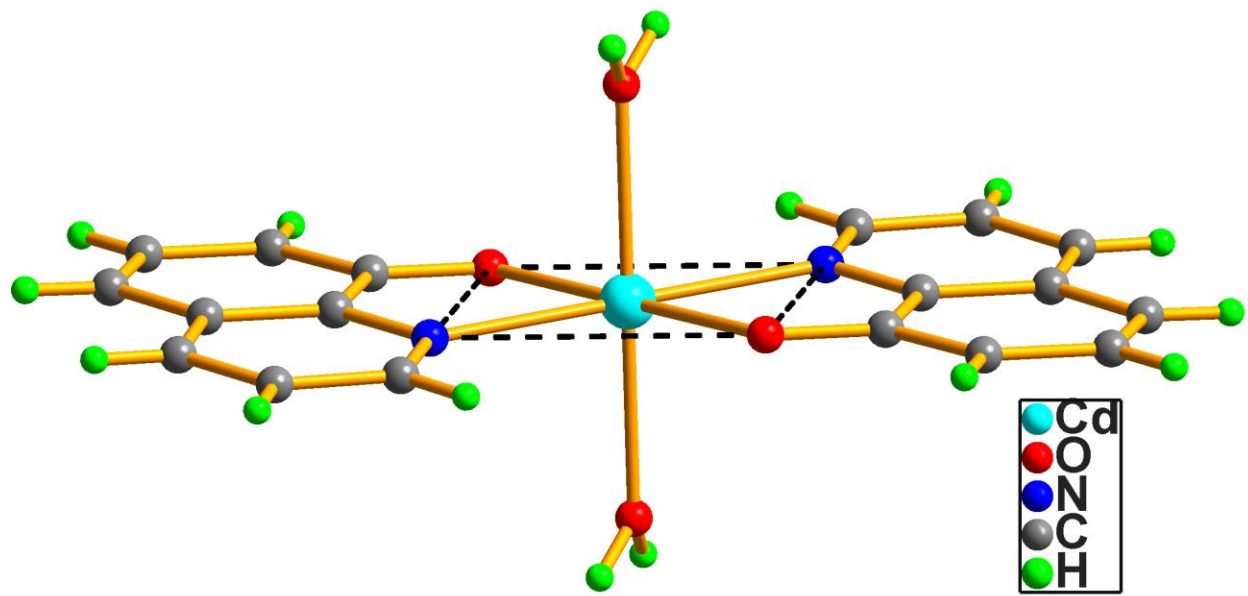
Fig. S7. The rectangular plane is represented by black dashed line constructed from two nitrogen and two oxygen atoms of Q^{1-}. The two water molecules are bonded to cadmium ion axially. The binding fashion of the Q and water in this complex is $\mu_1:\eta^1:\eta^1:\eta^1:\eta^1:\eta^1:\eta^1$.

Table S4. Non-covalent interaction in **1** (Hydrogen bonding table for the complex).

No.	Donor---H....Acceptor	[ARU]	D - H	H...A	D...A	D - H...A
1	Ow1 ---H1W....O1	[2656.01]	0.85(4)	1.89(4)	2.745(4)	178(5)
2	Ow1- --H2W....O1	[1565.01]	0.88	1.84	2.708(4)	171
3	C1---H1....Ow1	[3676.01]	0.93	2.52	3.397(5)	157

Translation of ARU-Code to CIF and Equivalent Position Code
===
  [1565.] =   x,1+y,z
  [2656.] =   1-x,1/2+y,3/2-z
  [3676.] =   1-x,2-y,1-z
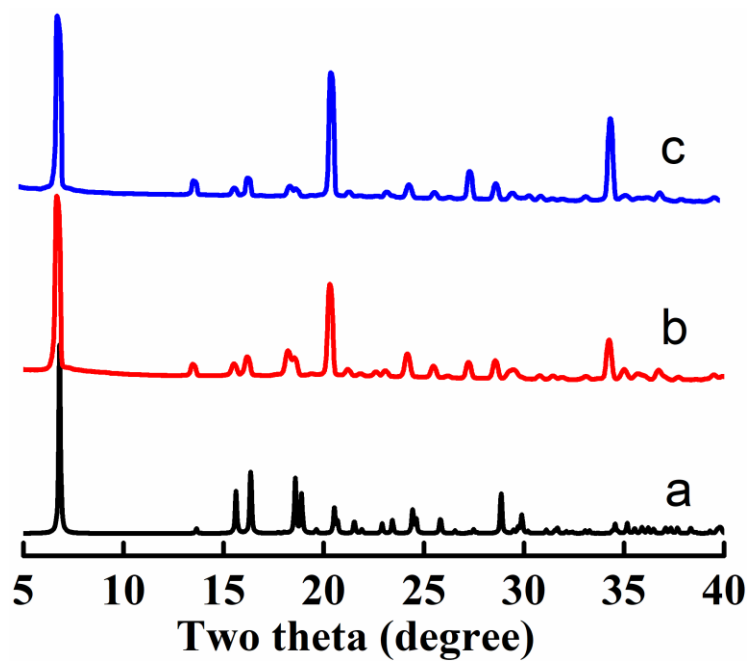
Fig. S8. (a) Simulated PXRD pattern of **1**, (b) as-synthesized PXRD pattern of **1,** (c) the PXRD pattern of **1** after keeping it in water for one day.
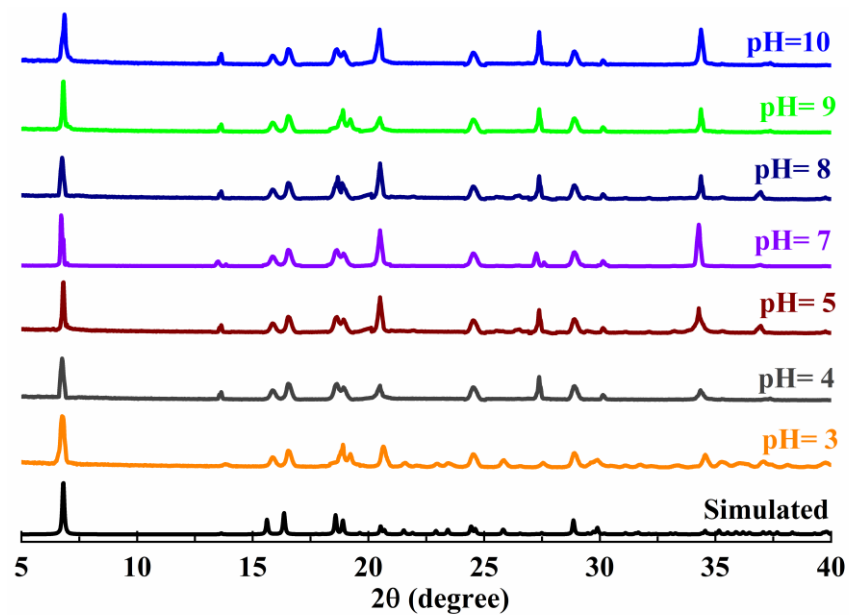
Fig. S9. PXRD pattern of compound **1** at 298 K after keeping in various acidic and basic solutions for 3 h.
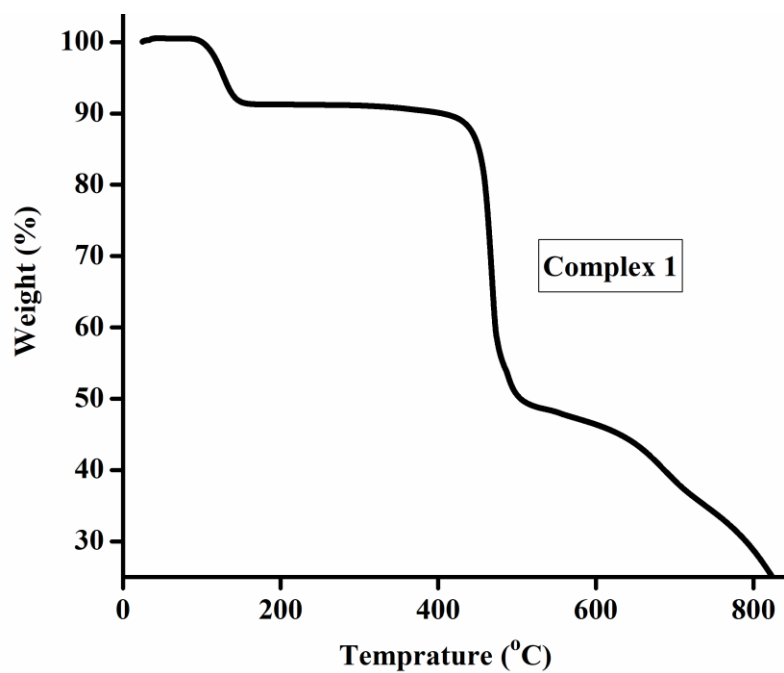
Fig. S10. TGA spectrum of **1**.
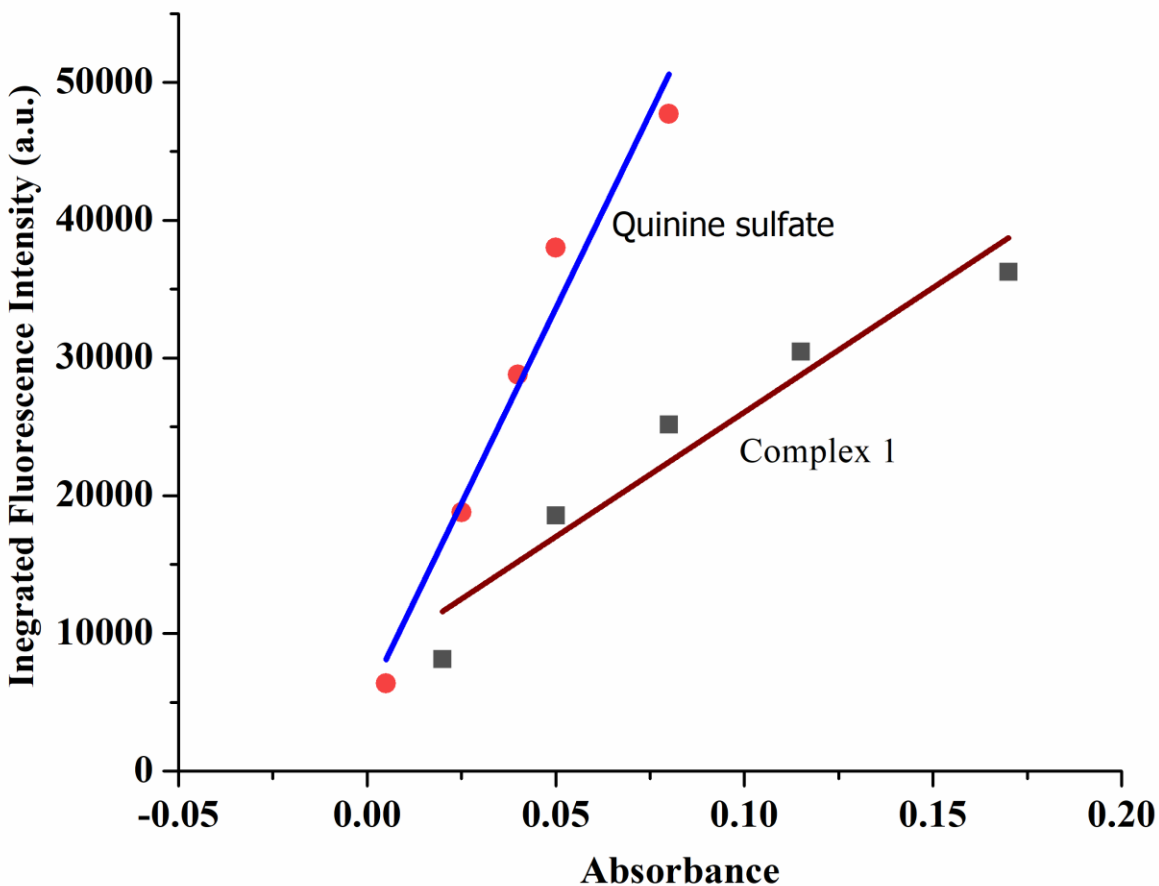
Fig. S11. The Plot of integrated fluorescence intensity versus the corresponding absorbance for quinine sulfate and studied complex **1**.

The fluorescence quantum yield of the complex **1** was determined by using the below equation and quinine sulfate as a standard compound. [15,16]

$$\Phi_1 = \Phi_{QS} \times \frac{(Gradient)_1}{(Gradient)_{QS}} \times \frac{n_1^2}{n_{QS}^2}$$

Where, Φ_{QS} and Φ_1 are the quantum yield of standard (quinine sulphate, $\Phi_{QS}=0.54$ in 0.1 M H_2SO_4) and studied complex **1** respectively. The "n" corresponds to the refractive index of the solution which is 1.33 in both 0.1 M H_2SO_4 and water. The gradient is obtained from the slope of the graph between integrated fluorescence luminescent (FL) intensity vs. absorbance of the standard and studied complex.

Compounds	Slope from integrated luminescent intensity versus corresponding absorbance	Refractive index	Quantum yield
Quinine sulphate	566430.33	1.33	0.54
Complex **1**	180821.18	1.33	Φ_1

$$\Phi_1 = \Phi_{QS} \times \frac{(Gradient)_1}{(Gradient)_{QS}} \times \frac{n_1^2}{n_{QS}^2}$$

$$\Phi_1 = 0.54 \times \frac{180821.18}{566430.33} \times \frac{(1.33)_1^2}{(1.33)_{QS}^2}$$

$$\Phi_1 = 0.54 \times 0.31923$$

$$\Phi_1 = 0.17$$
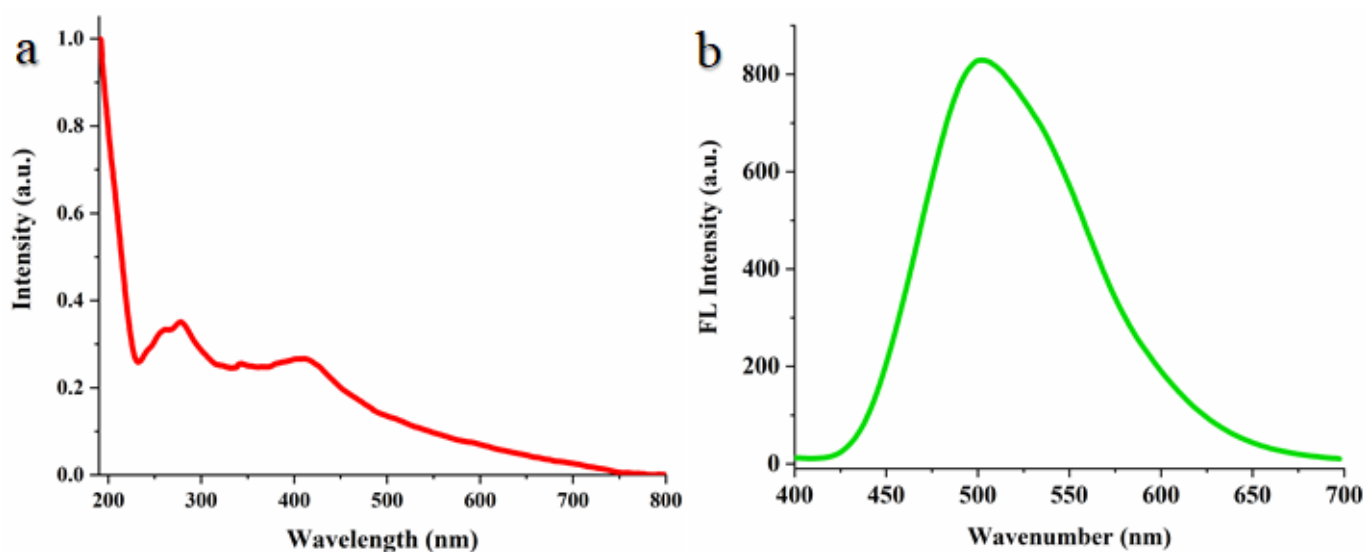
Fig. S12. (a) and (b) are the absorption and emission spectra of **1** in dispersed water medium.
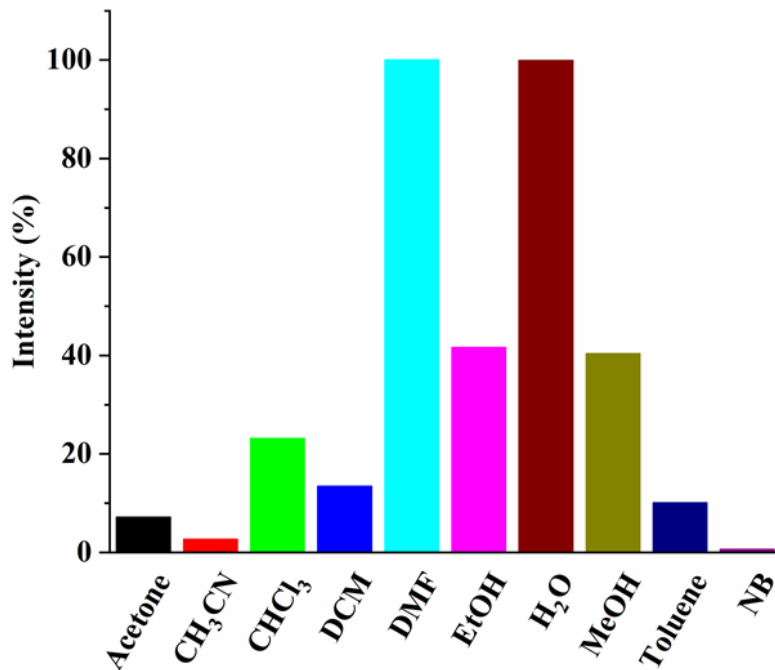
Fig. S13. The bar diagram of emission spectra of **1** in various solvents.
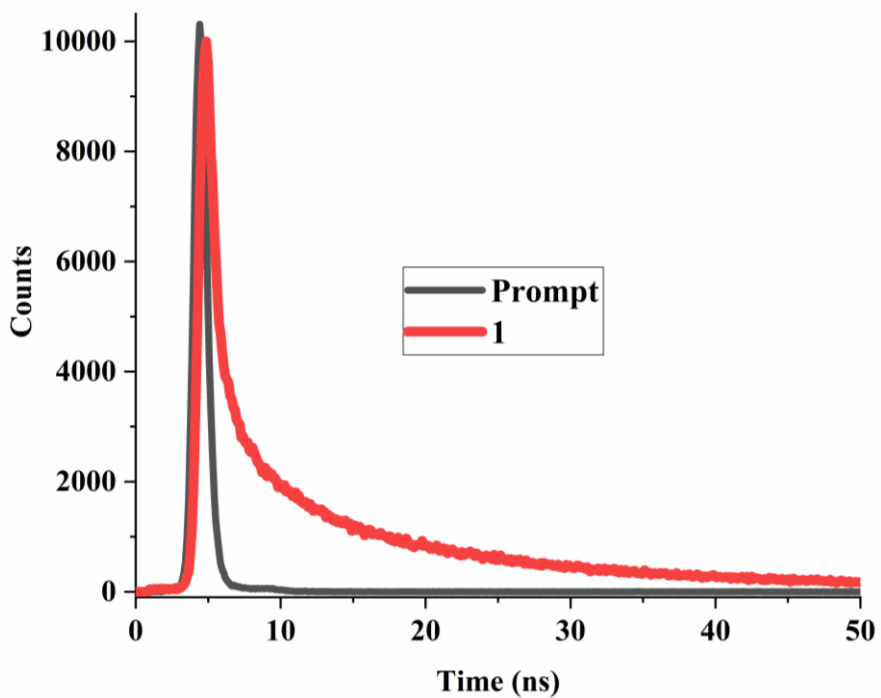
Fig. S14. Fluorescence exited state life time decay profile of compound **1** under excitation at 385 nm.
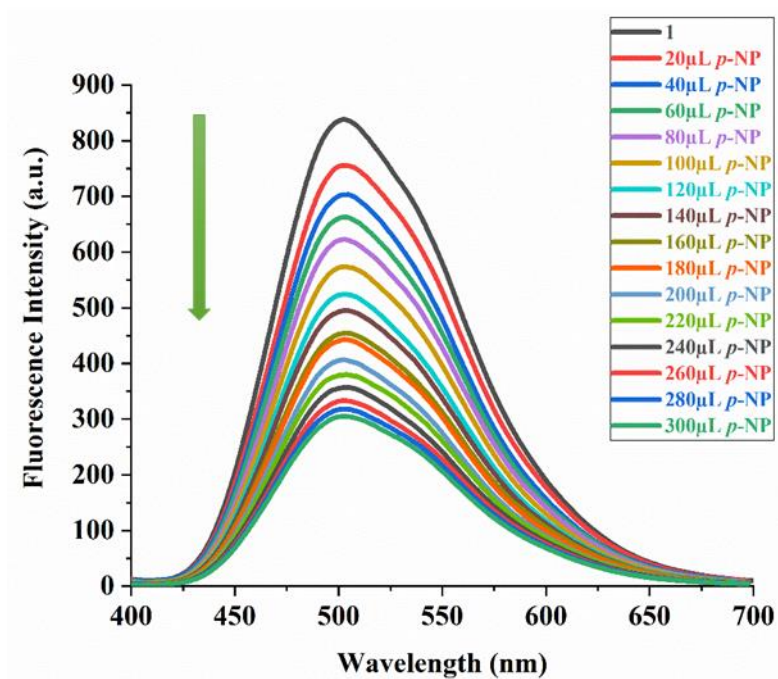
Fig. S15. Fluorescence titrations of **1** up on addition of *p*-nitrophenol (*p*-NP).
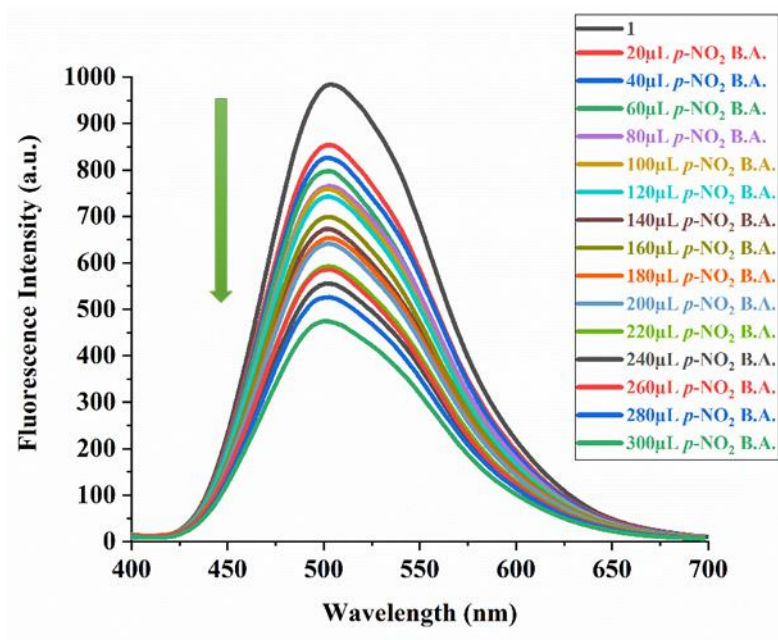
Fig. S16. Fluorescence titrations of **1** up on addition of *p*-nitro benzoic acid (*p*-NBA).
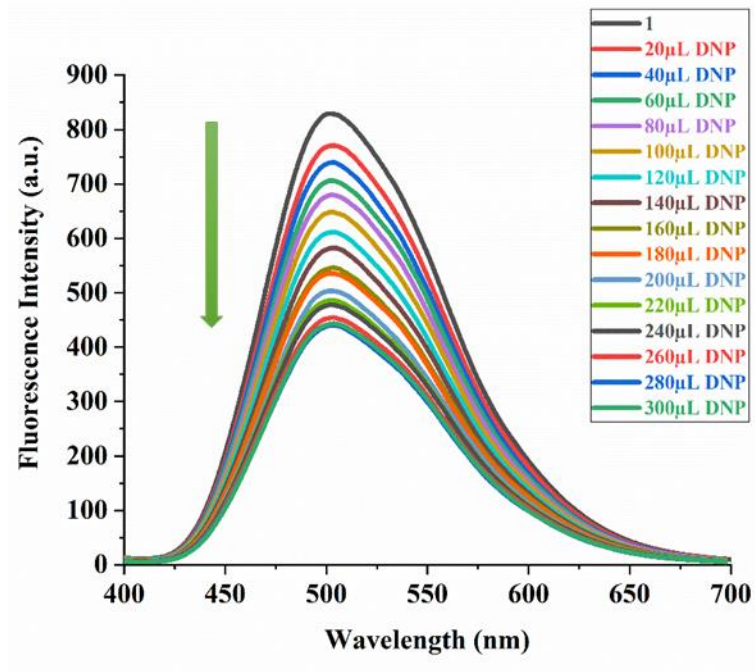
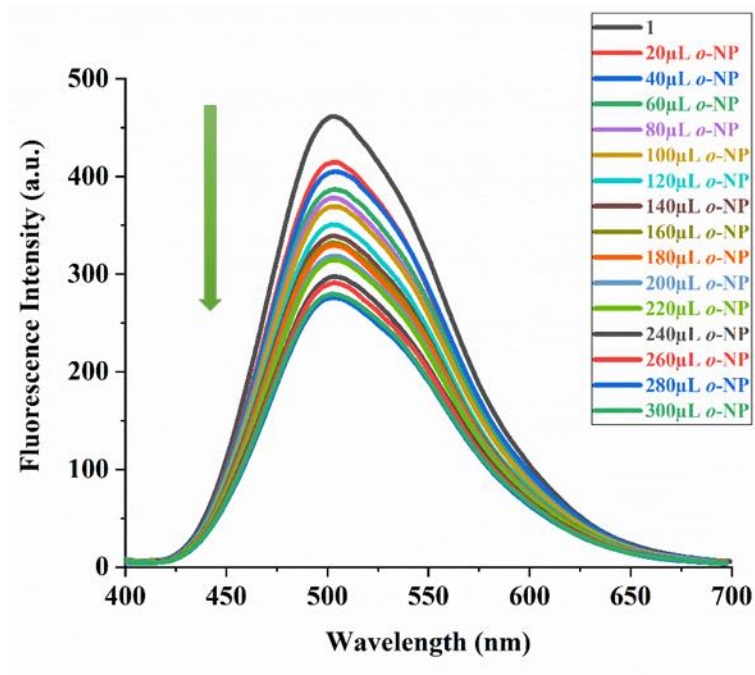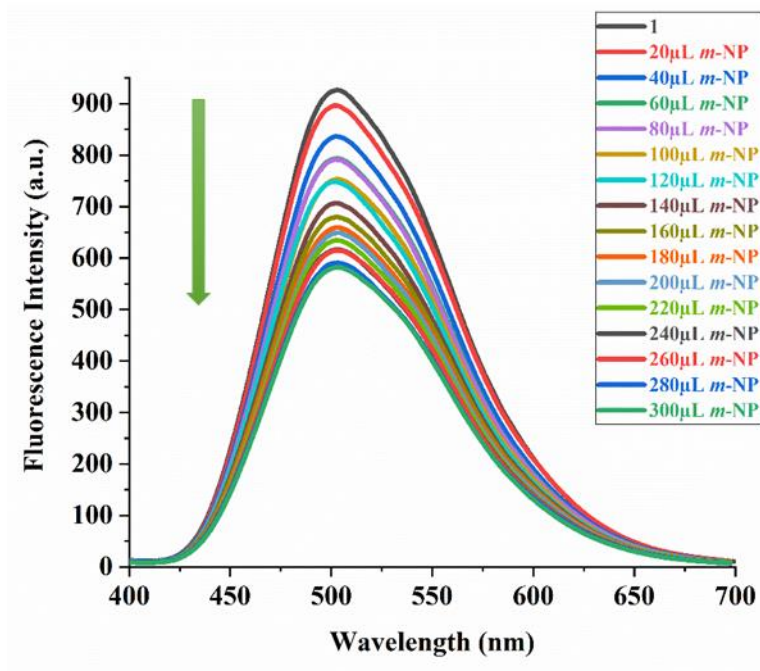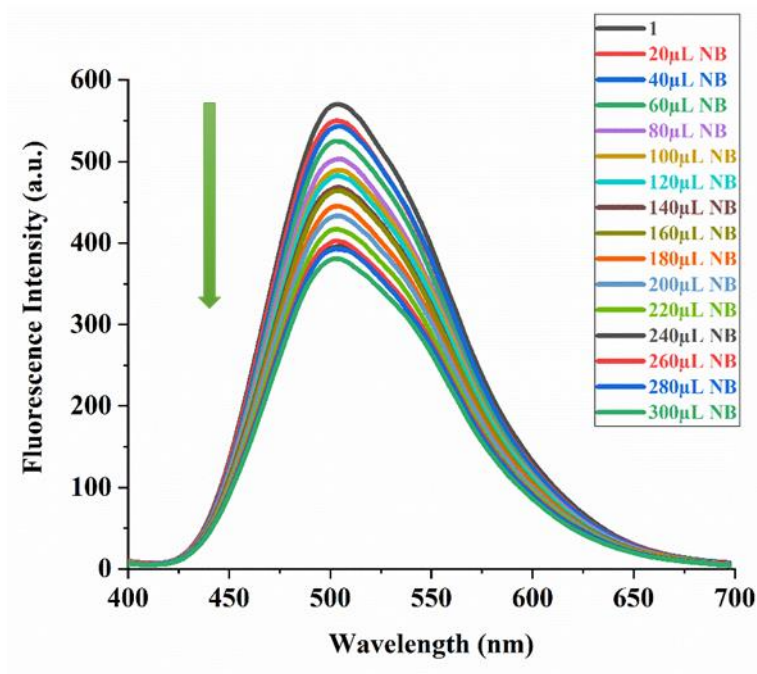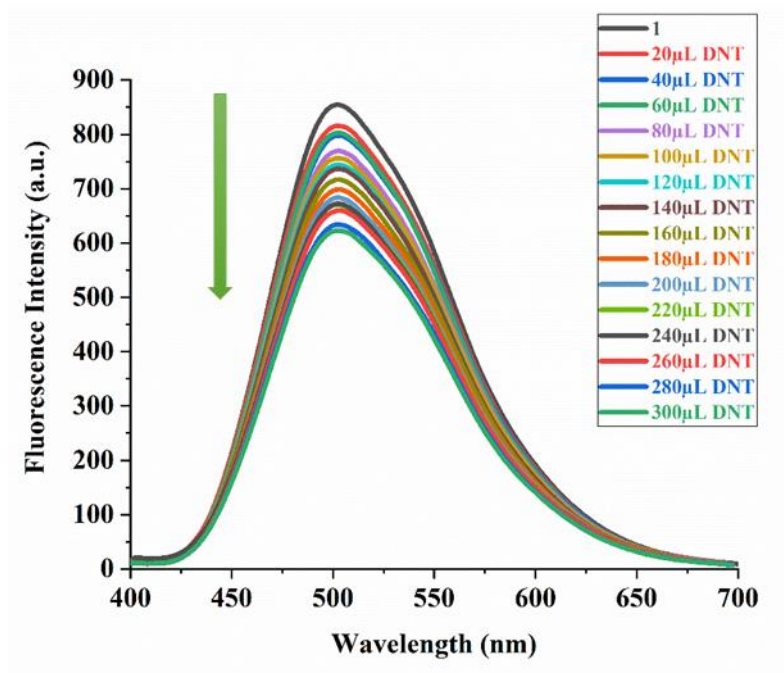**Fig. S17.** Fluorescence titrations of **1** up on addition of 2,4-dinitrophenol (2,4-DNP).

Fig. S18. Fluorescence titrations of **1** up on addition of *o*-nitrophenol (*o*-NP).

Fig. S19. Fluorescence titrations of **1** up on addition of *m*-nitrophenol (*m*-NP).

Fig. S20. Fluorescence titrations of **1** up on addition of nitrobenzene (NB).

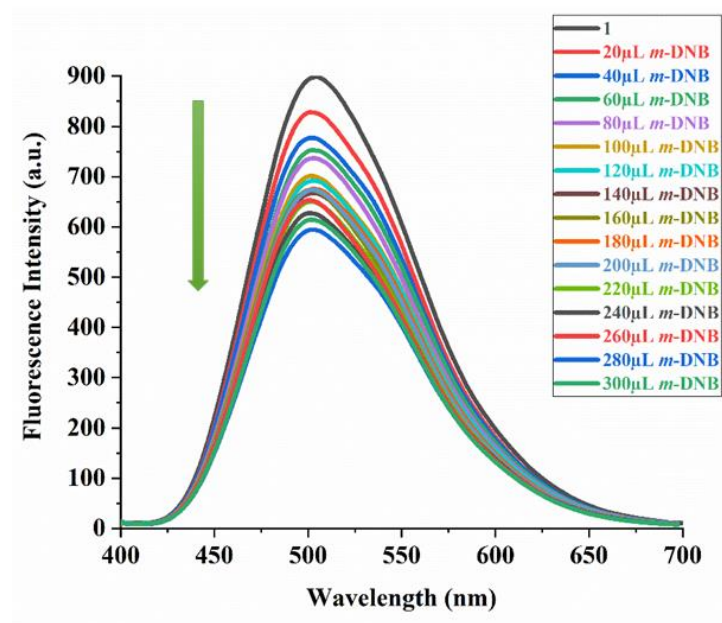**Fig. S21.** Fluorescence titrations of **1** up on addition of 2,4-dinitrotoluene (2,4-DNT).

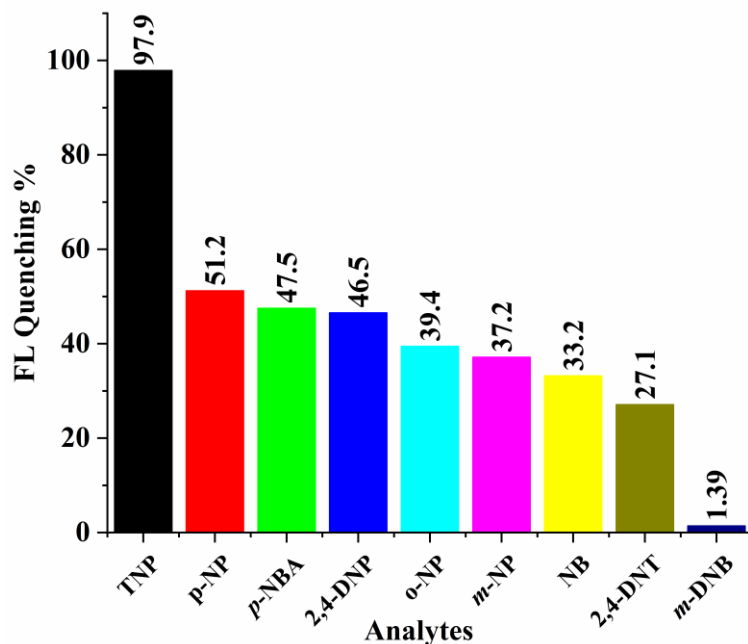**Fig. S22.** Fluorescence titrations of **1** up on addition of *m*-nitrobenzene (*m*-DNB).

Fig. S23. The quenching efficiency of different organic nitro analytes (ONAs) on the luminescent intensity of **1** in dispersed aqueous medium.
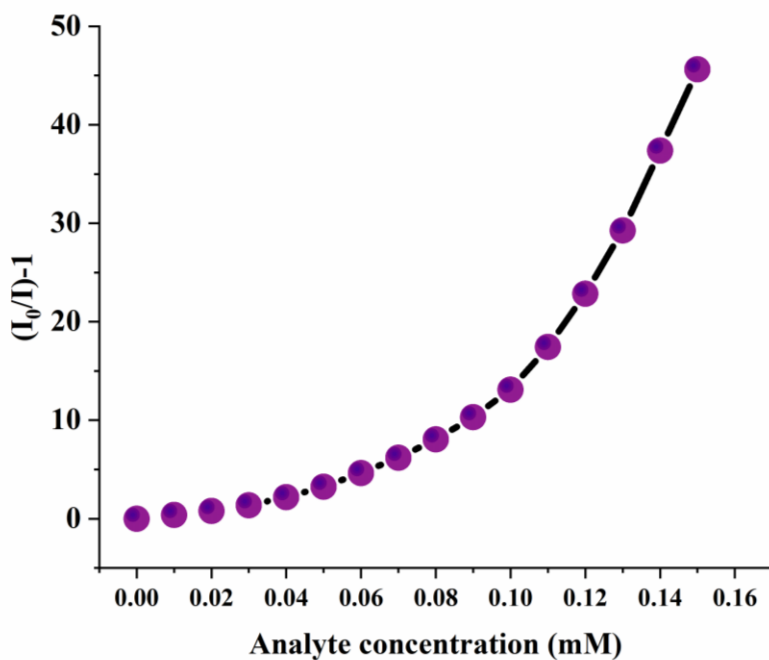

Fig. S24. The Stern-Volmer plot curvature for trinitrophenol (TNP) in the concentration range of 0-0.16 mM.
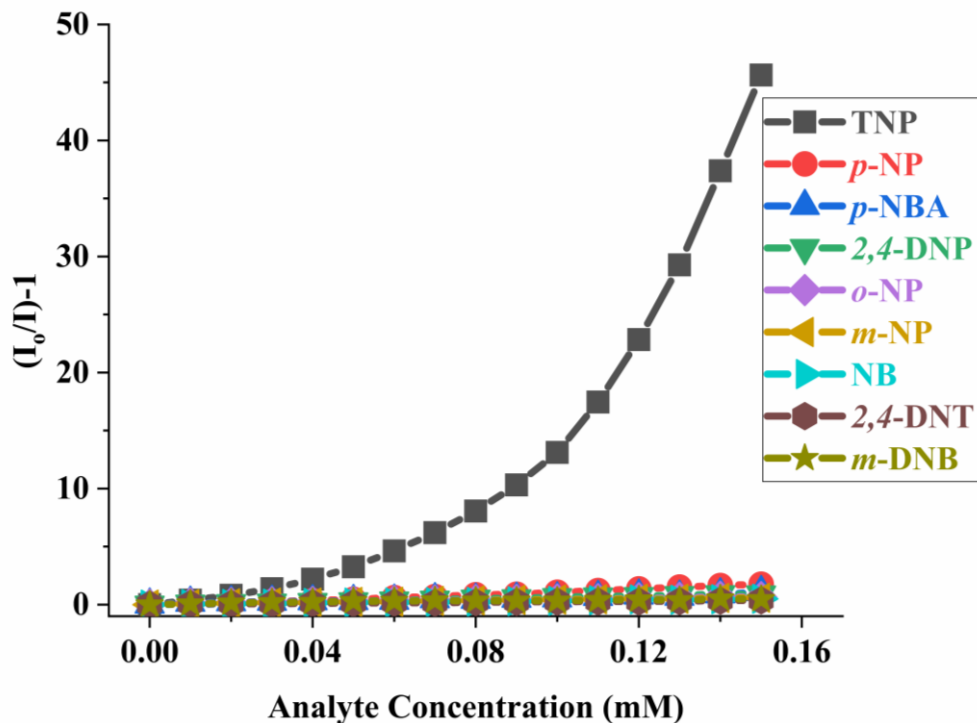
Fig. S25. The Stern-Volmer plot for all the investigated organic analytes in the concentration range of 0-0.16 mM.

Table S5. A literature data sheet for K_{sv} constants & LODs of various compound explored for the detection of toxic TNP.

Probe	Quenching constant K_{sv} (M^{-1})	Limit of Detection (LOD)	Medium	Ref.
1	5.3×10^4 M^{-1}	137 nM /59 ppb	H_2O	This work
Organic Probe				
Compound 1	3.43×10^3	3.48 ppm	H_2O	17
Nph-An	7×10^4	4.7×10^{-7} M	THF:H_2O (1:9)	18
Probe 1	1.76×10^5	5.5×10^{-7}	H_2O	19
Probe 2	9.87×10^4	M 3.7×10^{-6}		
Probe 3	1.65×10^4	5.3×10^{-6}		
PA	1.77×10^4	NA	H_2O	20
PF	3.9×10^4			
F1	3.94×10^4	5.7×10^{-7} M	H_2O	21
F2	2.1×10^4	9.3×10^{-7} M	H_2O	
bqbpxn	4.97×10^4	1.41 μM	H_2O	22
DNSA-SQ	NA	7×10^{-8} M	CH_3CN:H_2O (9:1)	23
MOF (Metal Organic Framework)				

{[Eu(HL)$_2$(H$_2$O)$_4$] 3·H$_2$O}n	6.76×10^4 M^{-1}	2.5 μM	H$_2$O	24
[Z$_r$$_6O_4(OH)_4(L)_6$]n	2.9 x 10^4	2.6 x 10^{-6} M	H$_2$O	25
[Tb(1,3,5-BTC)]n	3.4 x 10^4	8.1 x 10^{-8} M	EtOH	26
[Zn$_8$(ad)$_4$(BPDC)$_6$ (0.2Me$_2$NH$_2$)]·G	4.6 x 10^4	12.9 x 10^{-6} M	H$_2$O	27
[Zn$_2$(1,2-BDC)$_2$(BPDPE)$_2$]$_n$	1.99×10^4 M^{-1}	2.54 μM	H$_2$O	28
[Zn2(L2)(m1,5-dca)2(m1-dca)]n	1.54×10^4 M^{-1}	0.0199 ppm	H$_2$O/ DMF	29
BUT-12 BUT-13	3.1x10^5 5.1x10^5	23 ppb 10 ppb	H$_2$O	30
[Cd(NDC)0.5(PCA)]n	3.5 x 10^4	NA	CH$_3$CN	31
COF (Covalent Organic Framework)				
TfpBDH-COF	2.6 x 10^4	NA	IPA	32
Py-Azine COF	7.8 x 10^4	NA	CH$_3$CN	33
3D-Py-COF	3.1 x 10^4	NA	DMF	34
1	2.483 X 10^5	68 ppb	H$_2$O	35

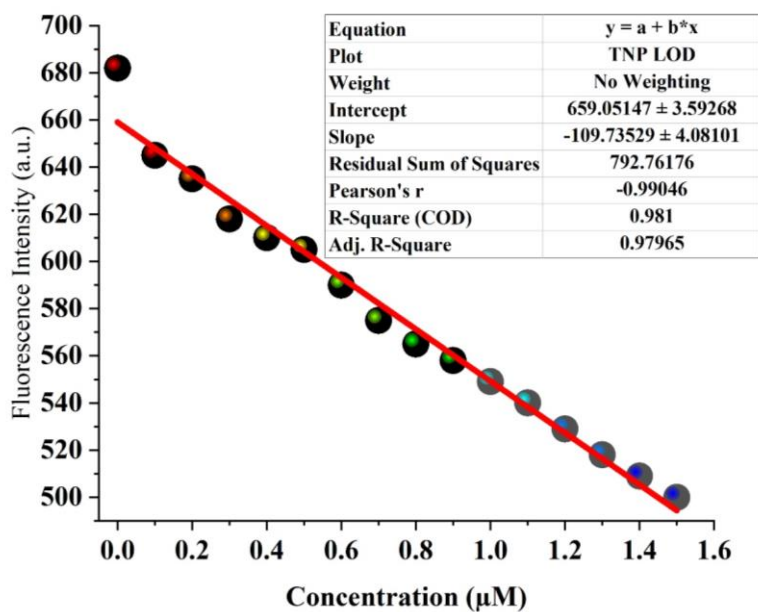| Equation	y = a + b*x
Plot	TNP LOD
Weight	No Weighting
Intercept	659.05147 ± 3.59268
Slope	-109.73529 ± 4.08101
Residual Sum of Squares	792.76176
Pearson's r	-0.99046
R-Square (COD)	0.981
Adj. R-Square	0.97965

Fig. S26. Linear fitting of fluorescence intensity of **1** upon addition of 10 μM of TNP solution (0–300 μL).

Table S6. LOD table: standard deviation (Fluorescence intensity) and limit of detection (LOD) calculations for **1** towards TNP.

Blank Readings (**1**)	Fluorescence Intensity (a.u.)
1	527.41152
2	516.62384
3	526.86504
4	522.77629
5	517.61323
Standard Deviation(σ)	5.034129958
Slope from Plot(M)	109.73μM^{-1}
Limit of Detection($3\sigma/M$)	0.137μM/137 nM
Limit of Detection(LOD)	0.059ppm/59 ppb
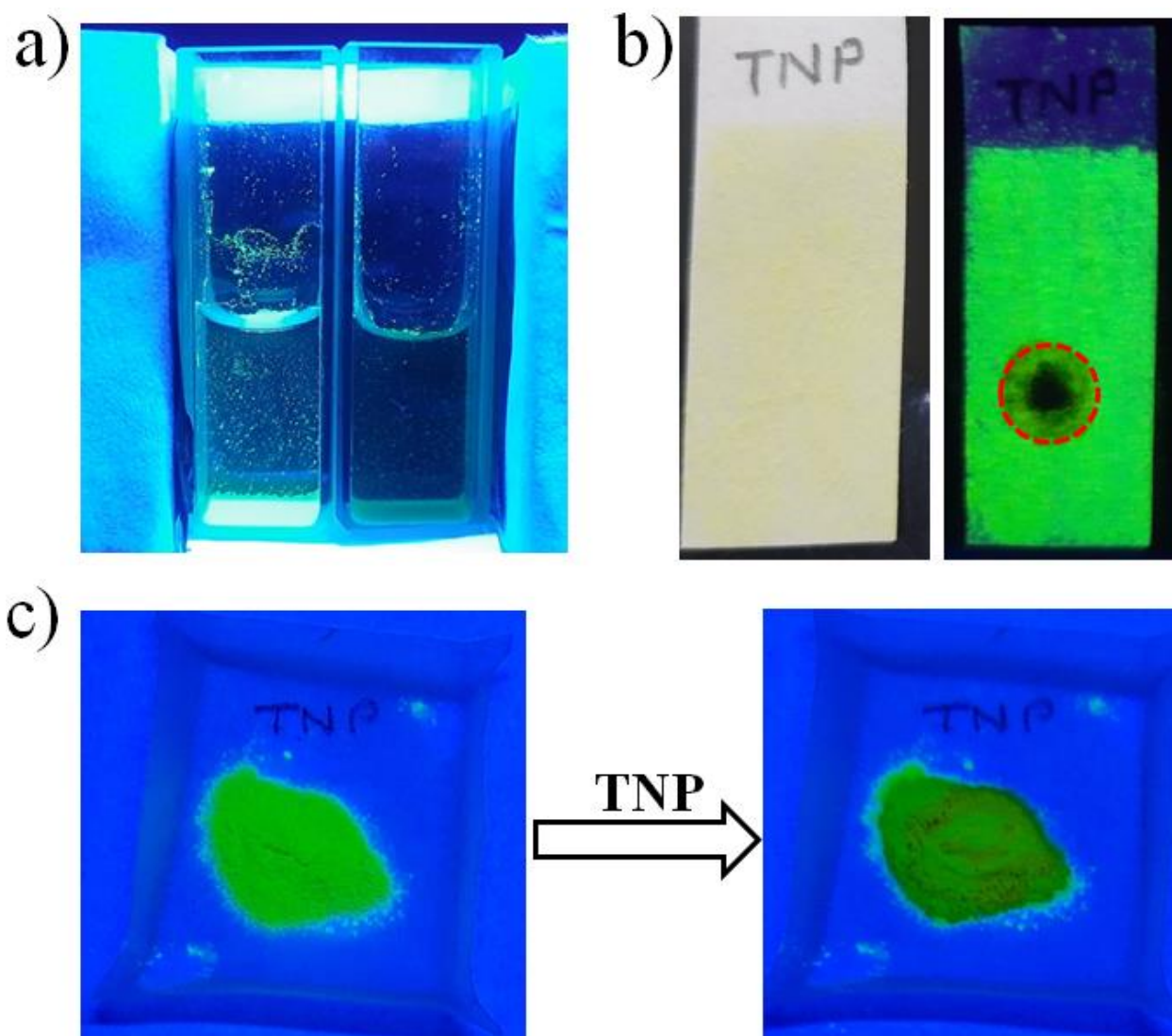
Fig. S27. The naked eye fluorescence turn–off process (a) Photograph of aqueous dispersed medium of **1** in cuvette before (left side) and after addition (right side) of TNP under UV light, (b) photograph of the strip paper encrusted with **1** under day light (left side) and after spotted with TNP (right side, red circle) under UV light and (c) photograph of bulk sample of **1** before (left side) and after addition of TNP (right side) under UV light .
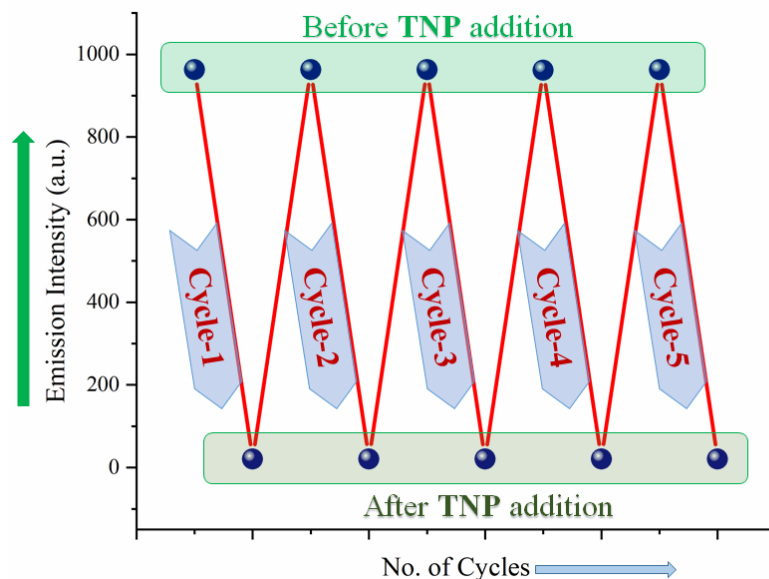
Fig. S28. Recycling behavior of **1** up to 5 consecutive cycles for the detection of TNP.
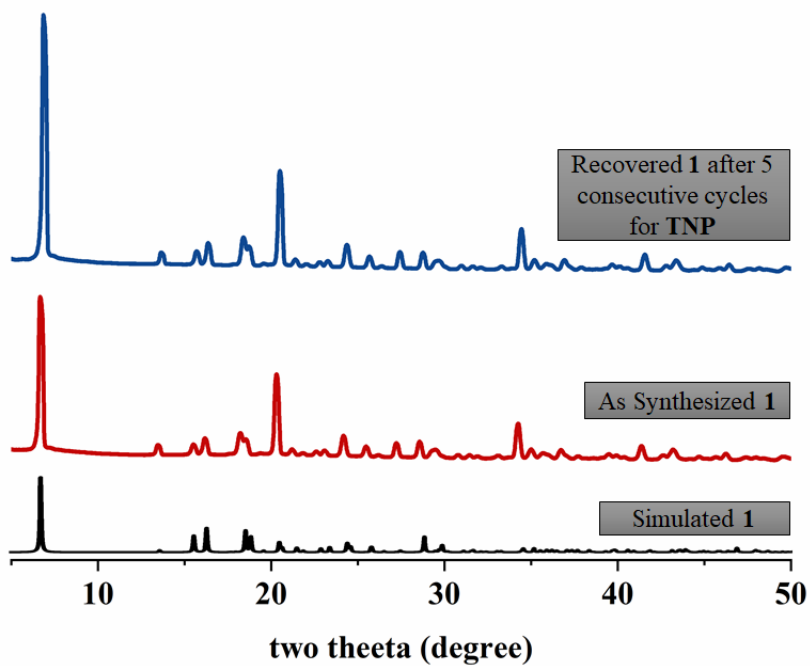
Fig. S29. Powder X-ray diffraction pattern of recovered **1** after five consecutive fluorescence sensing cycles for TNP along with the simulated and as-synthesized patterns.
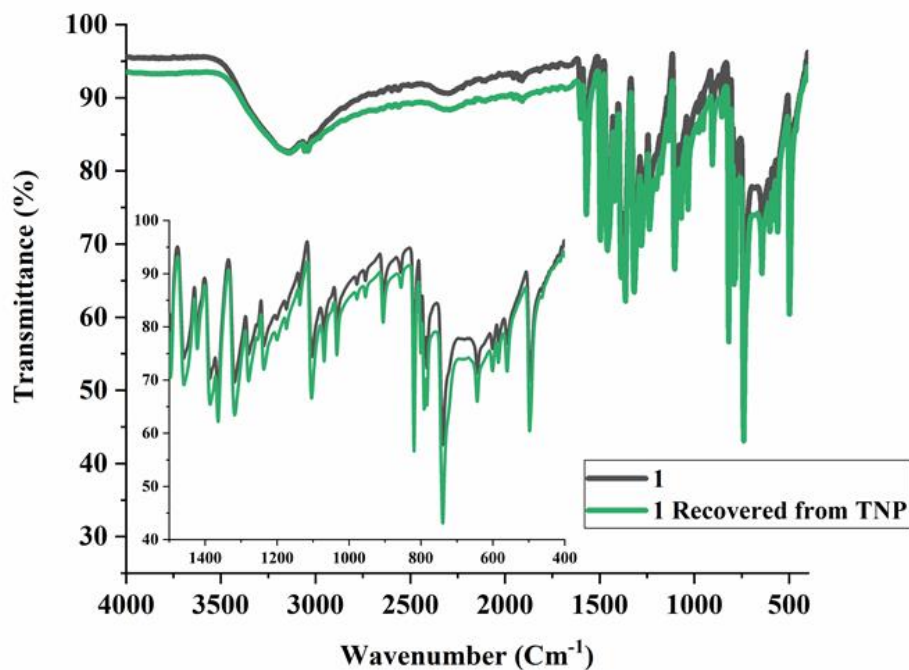
Fig. S30. FT-IR spectrum of as-synthesized **1** and recovered **1** after 5 cycles of TNP sensing study.
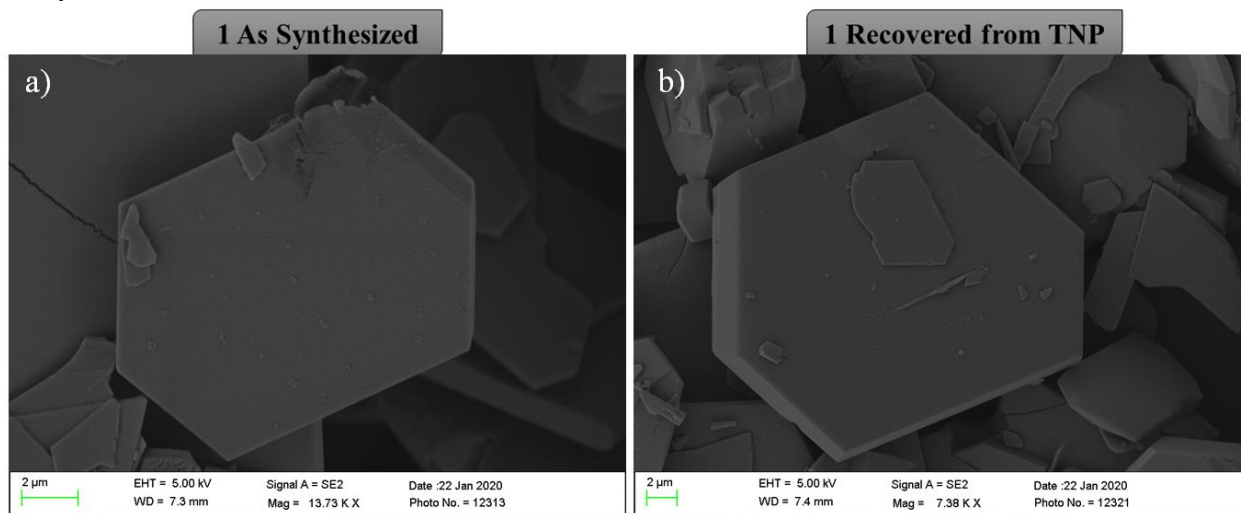

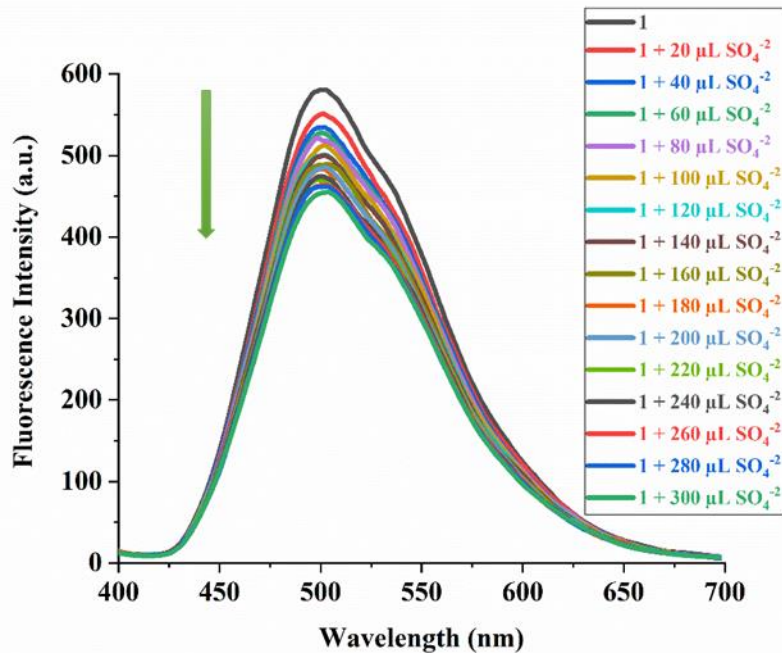**Fig. S31.** Morphology of **1** (a) as-synthesized and (b) after the TNP sensing experiment.

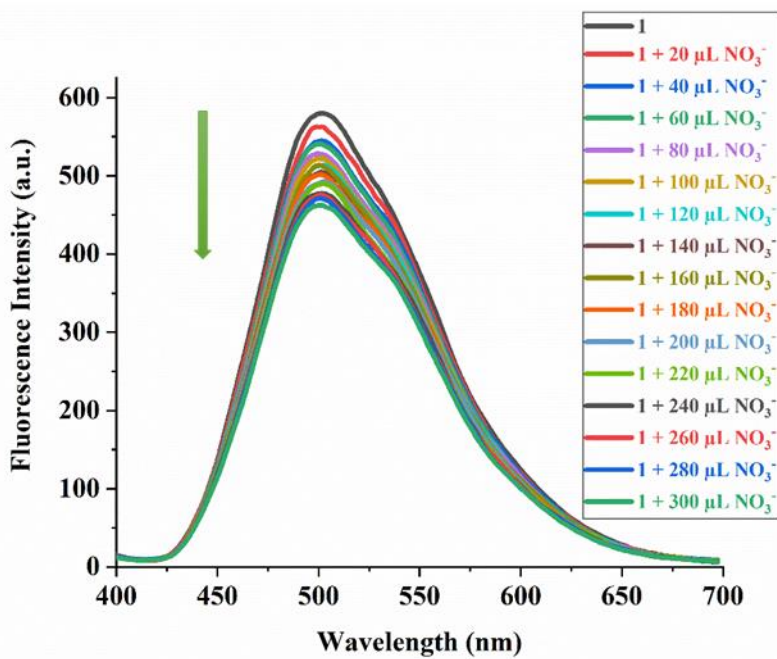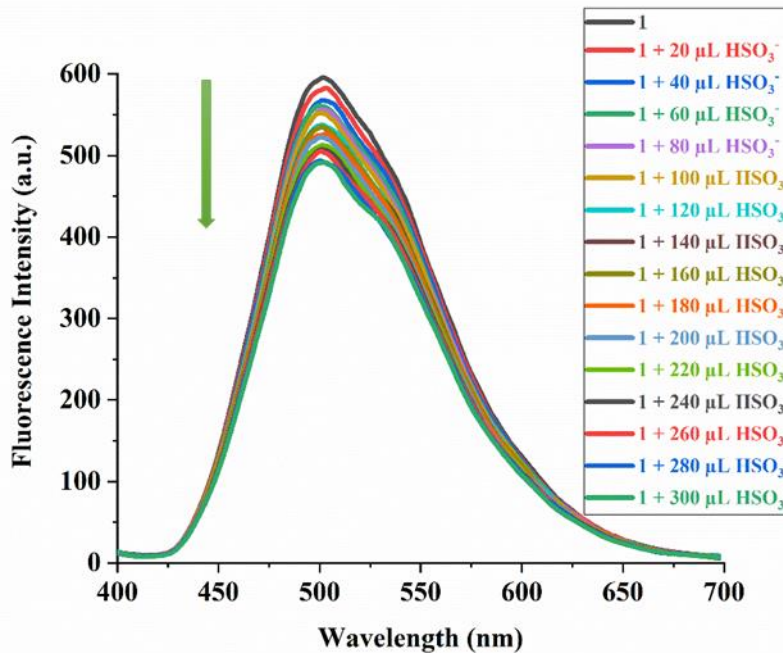**Fig. S32.** Fluorescence titrations of **1** upon addition of SO_4^{2-} ion in aqueous medium.

Fig. S33. Fluorescence titrations of **1** upon addition of NO_3^- ion in aqueous medium.

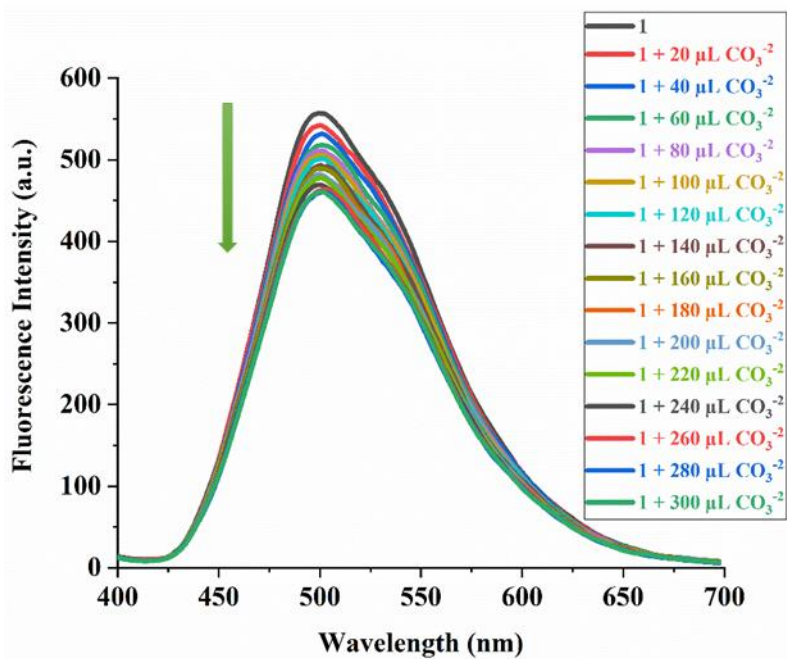**Fig. S34.** Fluorescence titrations of **1** upon addition of HSO_3^- ion in aqueous medium.

Fig. S35. Fluorescence titrations of **1** upon addition of CO_3^{2-} ion in aqueous medium.
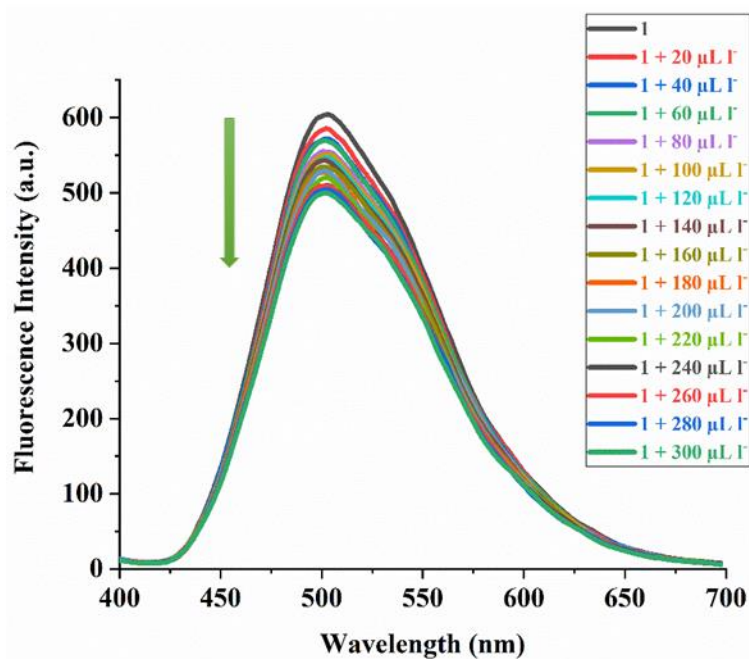
Fig. S36. Fluorescence titrations of **1** upon addition of I⁻ ion in aqueous medium.
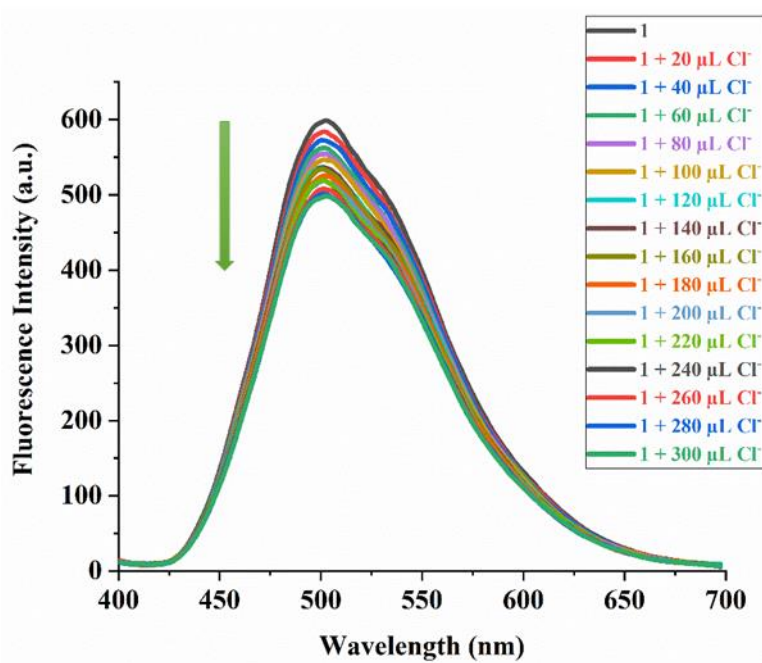

Fig. S37. Fluorescence titrations of **1** upon addition of Cl⁻ ion in aqueous medium.
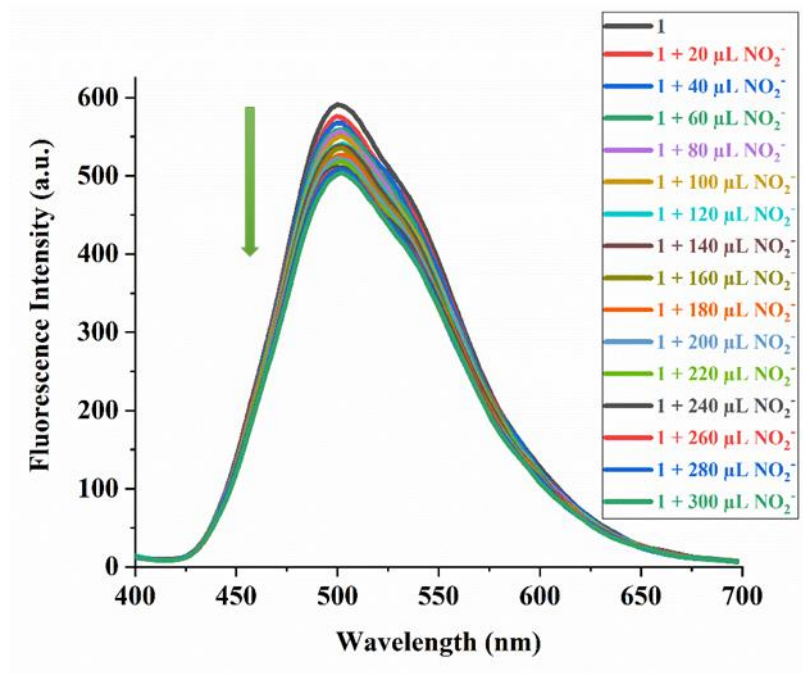
Fig. S38. Fluorescence titrations of **1** upon addition of NO_2^- ion in aqueous medium.
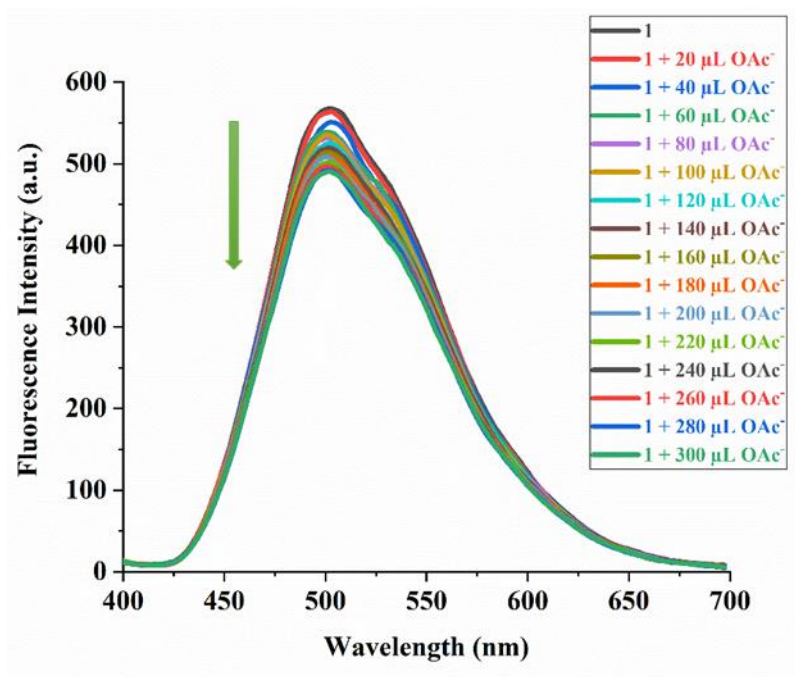

Fig. S39. Fluorescence titrations of **1** upon addition of acetate ion in aqueous medium.
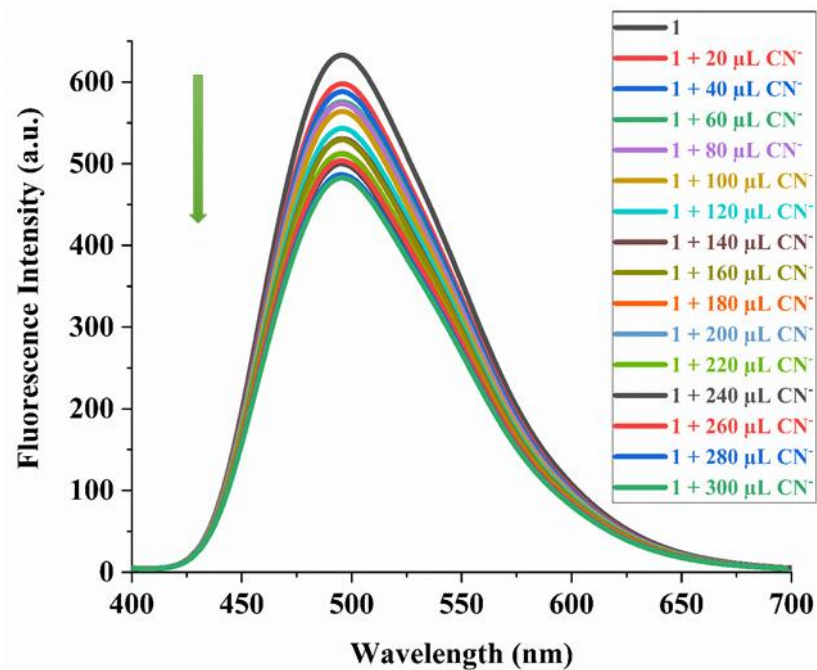
Fig. S40. Fluorescence titrations of **1** upon addition of CN$^-$ ion in aqueous medium.
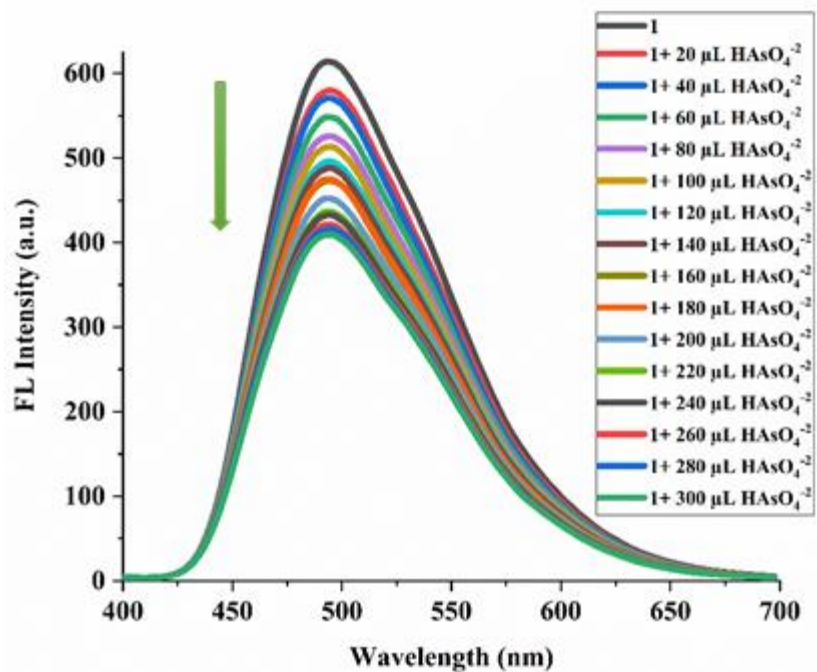

Fig. S41. Fluorescence titrations of **1** upon addition of arsenite (AsO$_2^-$) ion in aqueous medium.
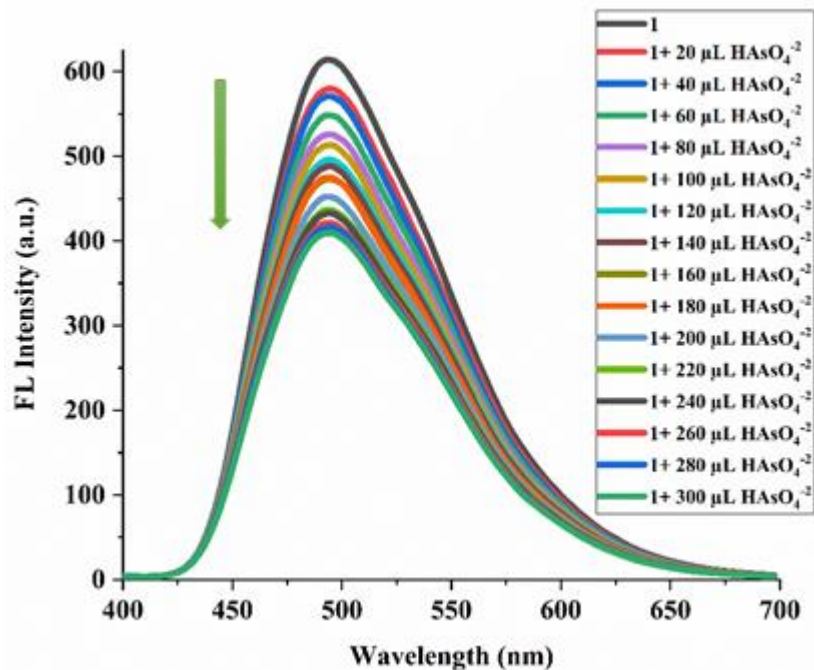
Fig. S42. Fluorescence titrations of **1** upon addition of arsenate ($HAsO_4^{-2}$) ion in aqueous medium.
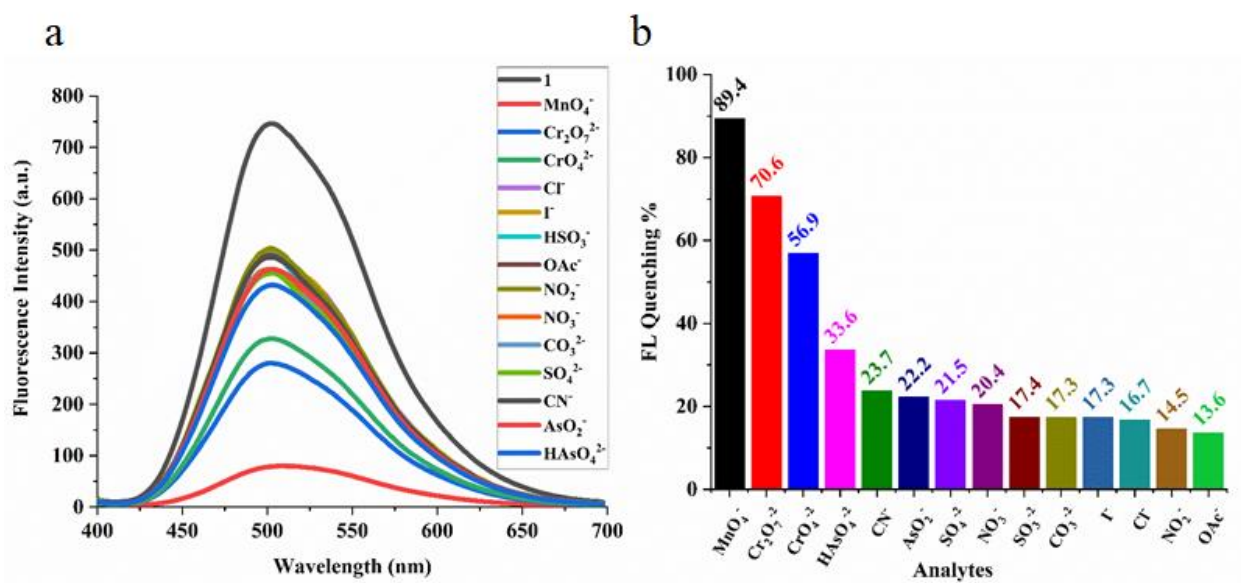

Fig. S43. (a) The fluorescence intensity of **1** after addition of 300 μL of various investigated anions and (b) the corresponding bar diagram represents the percentage of quenching.
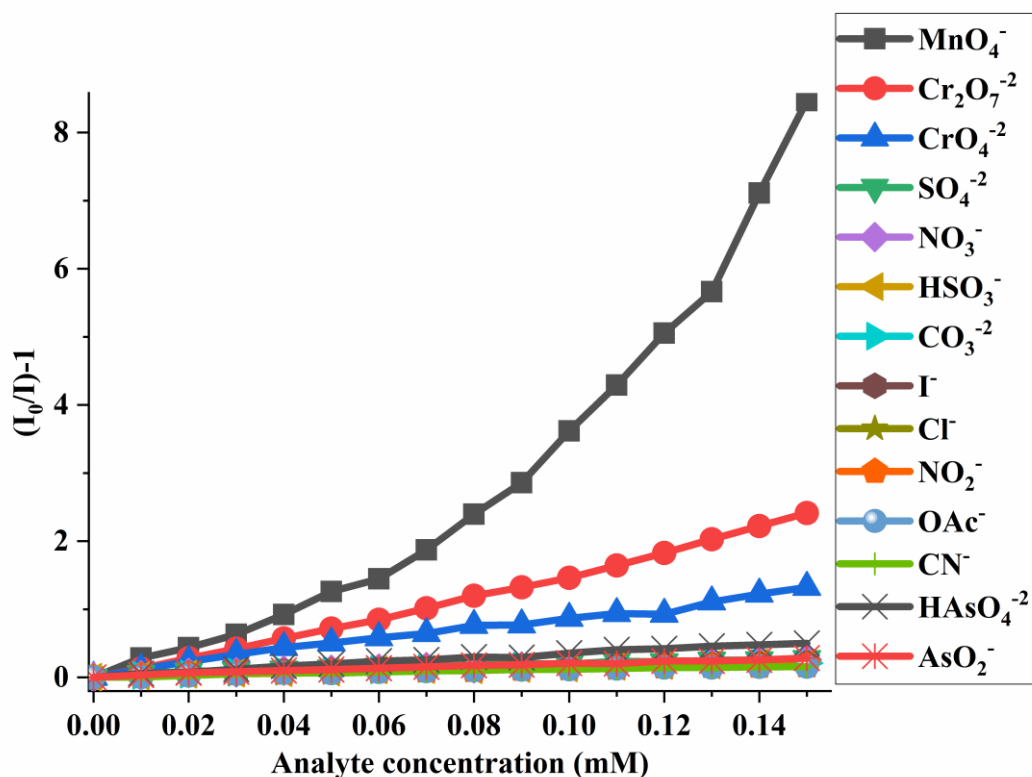
S33

Fig. S44. The Stern-Volmer plot for all the investigated anions in the concentration range of 0-0.16 mM.

Table S8. A literature data sheet for K_{sv} constants & LODs of various compounds explored for the detection of anions.

Probe	Oxo Anions	Quenching constant K_{sv} (M^{-1})	Limit of Detection (LOD)	Media	Ref.
		MOF/COF			
1	MnO_4^-	2.2×10^4 M^{-1}	141 nM/61 ppb	H_2O	This work
	$Cr_2O_7^{2-}$	1.4×10^4 M^{-1}	178 nM/78 ppb		
	CrO_4^{2-}	1.1×10^4 M^{-1}	219 nM/95 ppb		
TMU-41	MnO_4^-	3.2×10^5 M^{-1}	0.03 µM	H_2O	36
	$Cr_2O_7^{2-}$	1.0×10^6 M^{-1}	0.02 µM		
	CrO_4^{2-}	6.1×10^5 M^{-1}	0.03 µM		
$[Zn(modbc)_2]n$	MnO_4^-	7.44×10^4 M^{-1}	0.15 µM	DMF+ H_2O	37
	$Cr_2O_7^{2-}$	2.49×10^4 M^{-1}	0.43 µM		
	CrO_4^{2-}	1.18×10^4 M^{-1}	0.10 µM		
$\{[Zn_6Cl_6(2,2'-dbpt)_3] \cdot 6H_2O\}n$	MnO_4^-	2.0×10^5 M^{-1}	6.14 µM	(DMF:	38

	$Cr_2O_7^{2-}$	1.85×10^5 M^{-1}	13.64 μM	H$_2$O)	
	CrO_4^{2-}	5.89×10^4 M^{-1}	12.33 μM	(1:1)	
{[Zn(bpdc)(Cz-3,6-bpy)]·DMF·H$_2$O}$_n$	MnO_4^-	6.42×10^3 M^{-1}	2.18 μM	DMF	39
	$Cr_2O_7^{2-}$	5.79×10^3 M^{-1}	0.94 μM		
	CrO_4^{2-}	3.40×10^3 M^{-1}	2.29 μM		
USTC-5	MnO_4^-	1.92×10^4 M^{-1}	23.40 μM	H$_2$O	40
	$Cr_2O_7^{2-}$	1.25×10^4 M^{-1}	1.45 μM		
	CrO_4^{2-}	1.34×10^4 M^{-1}	11.40 μM		
{[Cd (ttpe)(H2O)(ip)]•4H2O•DMAC}n	MnO_4^-	6.45×10^4 M^{-1}	0.34 μM	H$_2$O	41
	$Cr_2O_7^{2-}$	4.23×10^4 M^{-1}	0.09 μM		
	CrO_4^{2-}	2.47×10^4 M^{-1}	0.10 μM		
[Ni2(μ2-OH)(azdc)(tpim)](NO3)·6DMA·6MeOH	MnO_4^-	3.66×10^3 M^{-1}	0.26 μM	H$_2$O	42
	$Cr_2O_7^{2-}$	1.31×10^4 M^{-1}	0.95 μM		
	CrO_4^{2-}	7.9×10^3 M^{-1}	0.30 μM		
COF-TT	MnO_4^-	1.5×10^4	3.20×10^{-4} M		43
	$Cr_2O_7^{2-}$	1.4×10^4	3.43×10^{-4} M	H$_2$O	
	CrO_4^{2-}	1.4×10^4	3.43×10^{-4} M		

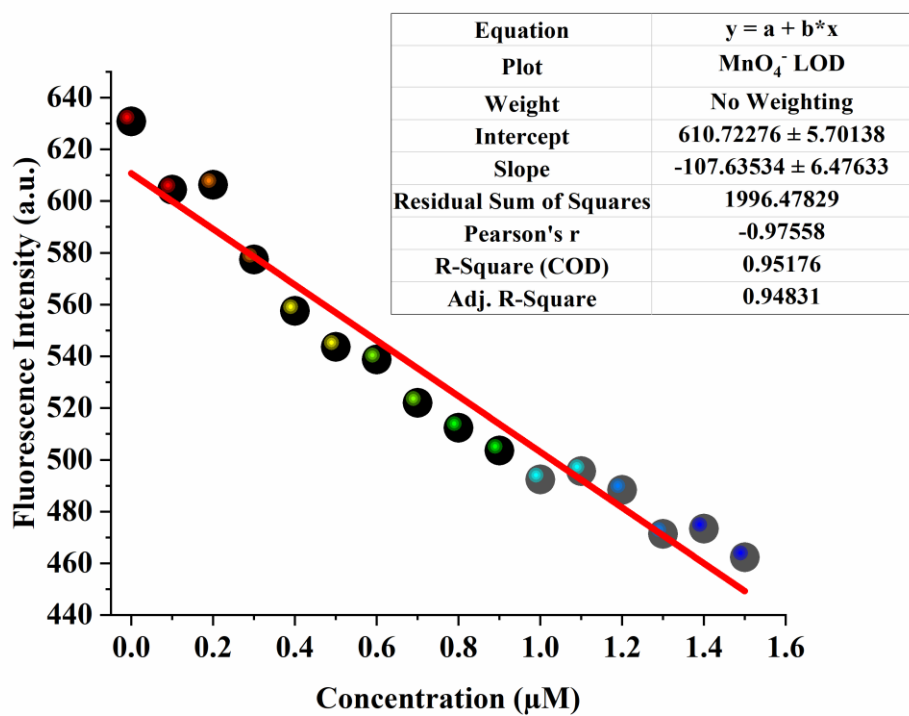| Equation	$y = a + b*x$
Plot	MnO_4^- LOD
Weight	No Weighting
Intercept	610.72276 ± 5.70138
Slope	-107.63534 ± 6.47633
Residual Sum of Squares	1996.47829
Pearson's r	-0.97558
R-Square (COD)	0.95176
Adj. R-Square	0.94831

Fig. S45. Linear fitting of fluorescence intensity of **1** upon addition of 10 μM of MnO$_4^-$ solution (0 –300 μL).

Table S9. LOD table: standard deviation (Fluorescence intensity) and limit of detection (LOD) calculations for **1** towards MnO_4^-.

Blank Readings (**1**)	Fluorescence Intensity (a.u.)
1	527.41152
2	516.62384
3	526.86504
4	522.77629
5	517.61323
Standard Deviation (σ)	5.034129958
Slope from Plot (*M*)	107.63 μM^{-1}
Limit of Detection($3\sigma/M$)	0.140 μM
Limit of Detection(LOD)	141 nM/61 ppb

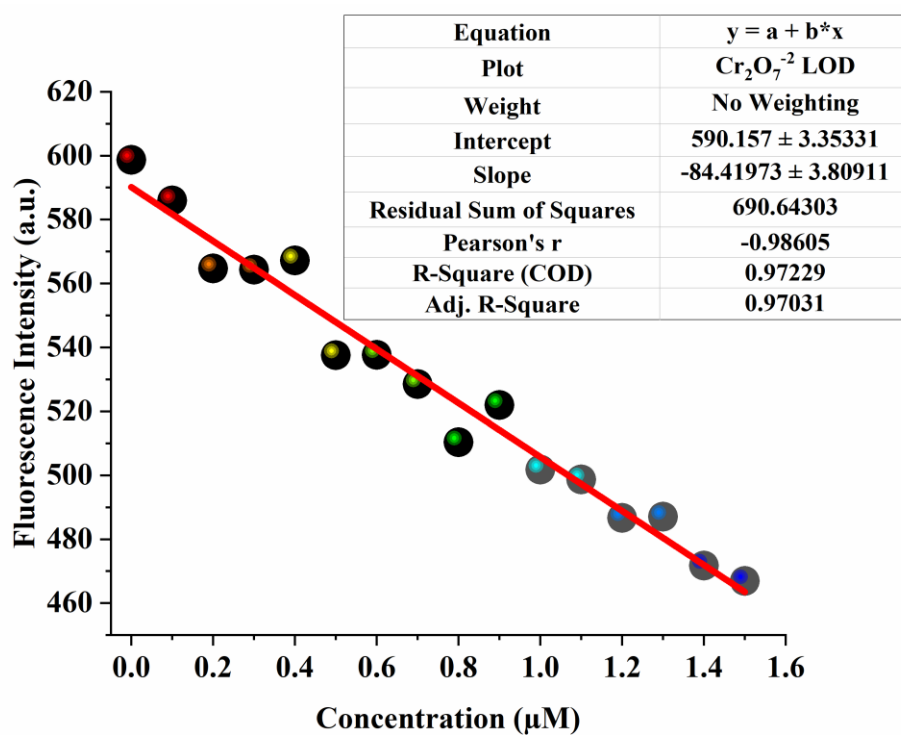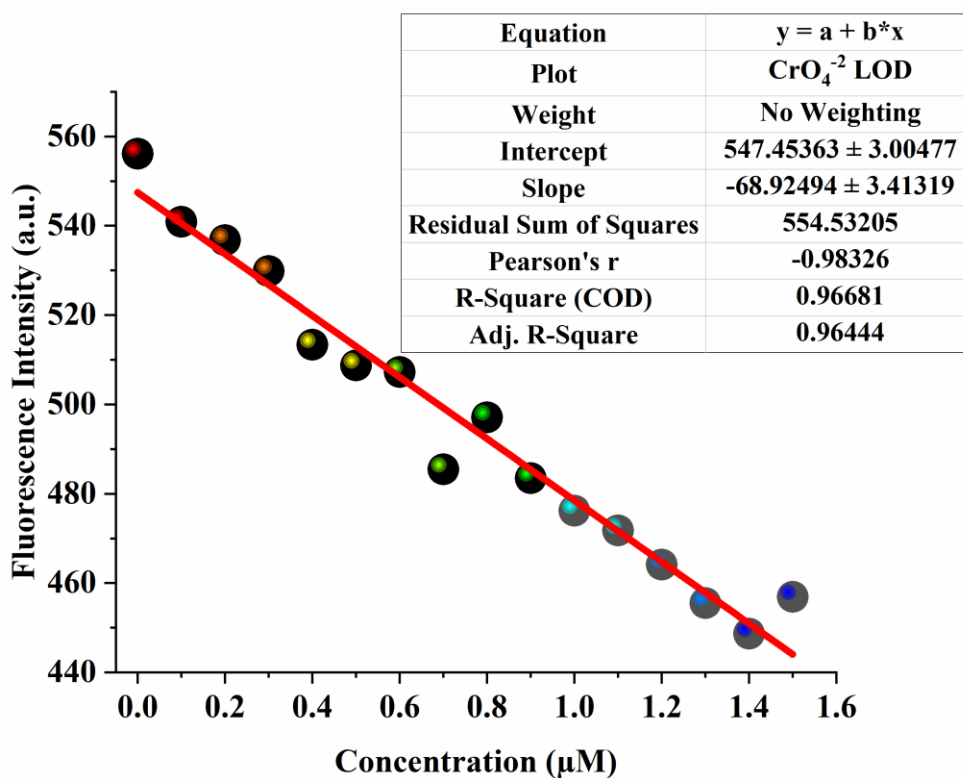| Equation	$y = a + b*x$
Plot	$Cr_2O_7^{-2}$ **LOD**
Weight	No Weighting
Intercept	590.157 ± 3.35331
Slope	-84.41973 ± 3.80911
Residual Sum of Squares	690.64303
Pearson's r	-0.98605
R-Square (COD)	0.97229
Adj. R-Square	0.97031

Fig. S46. Linear fitting of fluorescence intensity of **1** upon addition of 10 μM of $Cr_2O_7^{2-}$ solution (0 –300 μL).

Table S10. LOD table: standard deviation (Fluorescence intensity) and limit of detection (LOD) calculations for 1 towards $Cr_2O_7^{2-}$.

Blank Readings (1)	Fluorescence Intensity (a.u.)
1	527.41152
2	516.62384
3	526.86504
4	522.77629
5	517.61323
Standard Deviation(σ)	5.034129958
Slope from Plot (M)	84.41μM^{-1}
Limit of Detection($3\sigma/M$)	0.178 μM
Limit of Detection(LOD)	178 nM/78 ppb

Equation	$y = a + b*x$
Plot	CrO_4^{-2} LOD
Weight	No Weighting
Intercept	547.45363 ± 3.00477
Slope	-68.92494 ± 3.41319
Residual Sum of Squares	554.53205
Pearson's r	-0.98326
R-Square (COD)	0.96681
Adj. R-Square	0.96444

Fig. S47. Linear fitting of fluorescence intensity of **1** upon addition of 10 μM of CrO_4^{2-} solution (0 –300 μL).

Table S11. LOD table: standard deviation (Fluorescence intensity) and limit of detection (LOD) calculations for 1 towards CrO_4^{2-}.

Blank Readings (1)	Fluorescence Intensity (a.u.)
1	527.41152
2	516.62384
3	526.86504
4	522.77629
5	517.61323
Standard Deviation(σ)	5.034129958
Slope from Plot (M)	68.92μM^{-1}
Limit of Detection($3\sigma/M$)	0.219 μM
Limit of Detection(LOD)	219 nM/95 ppb
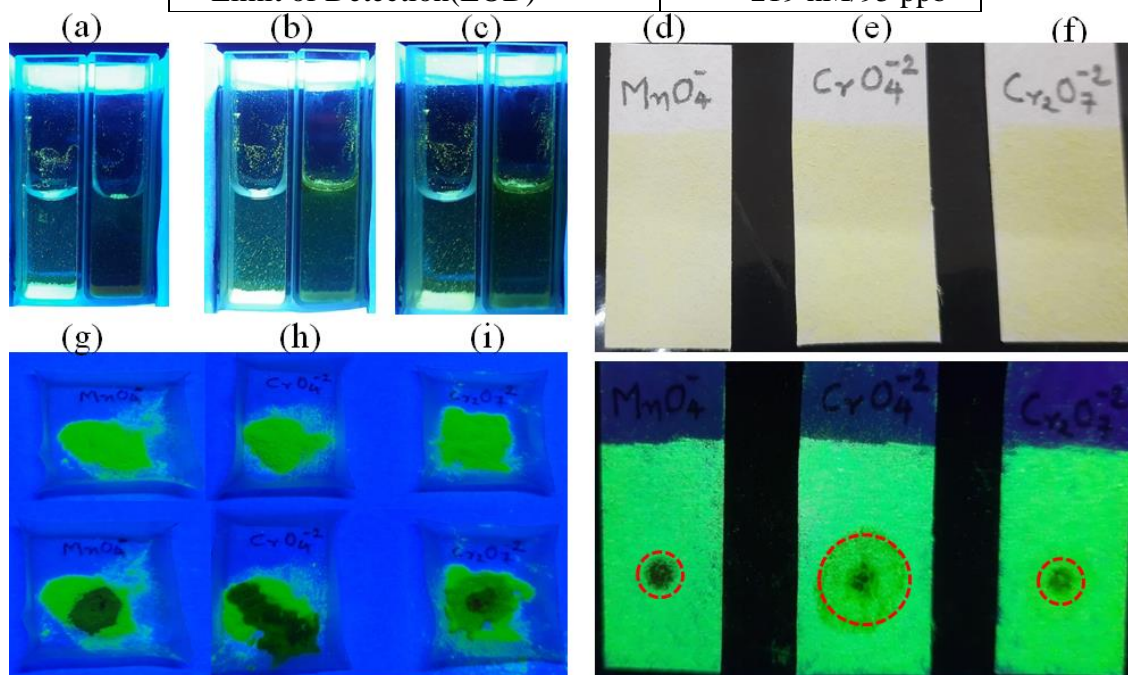
Fig. S48. The naked eye fluorescence turn–off process under UV light: Photograph of aqueous dispersed medium of **1** before (left side in each set) and after addition (right side in each set) of (a) MnO_4^-, (b) CrO_4^{2-} and (c) $Cr_2O_7^{2-}$ under UV light; Photograph of the strip paper encrusted with **1** before (top in each set) and after spotted with (d) MnO_4^-, (e) CrO_4^{2-} and (f) $Cr_2O_7^{2-}$ (bottom, red circle in each set) under UV light and; Photograph of bulk sample of **1** before (top in each set)) and after addition of (g) MnO_4^-, (h) CrO_4^{2-} and (i) $Cr_2O_7^{2-}$ (bottom in each set).
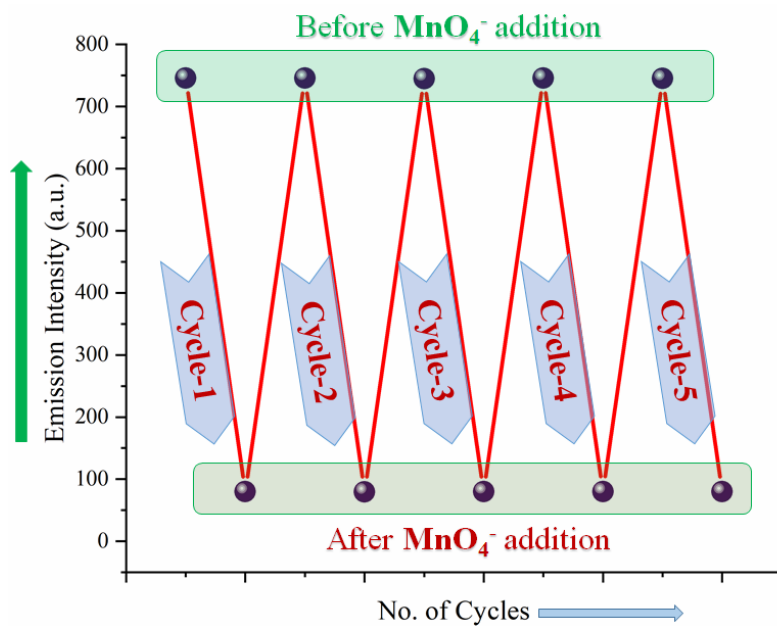
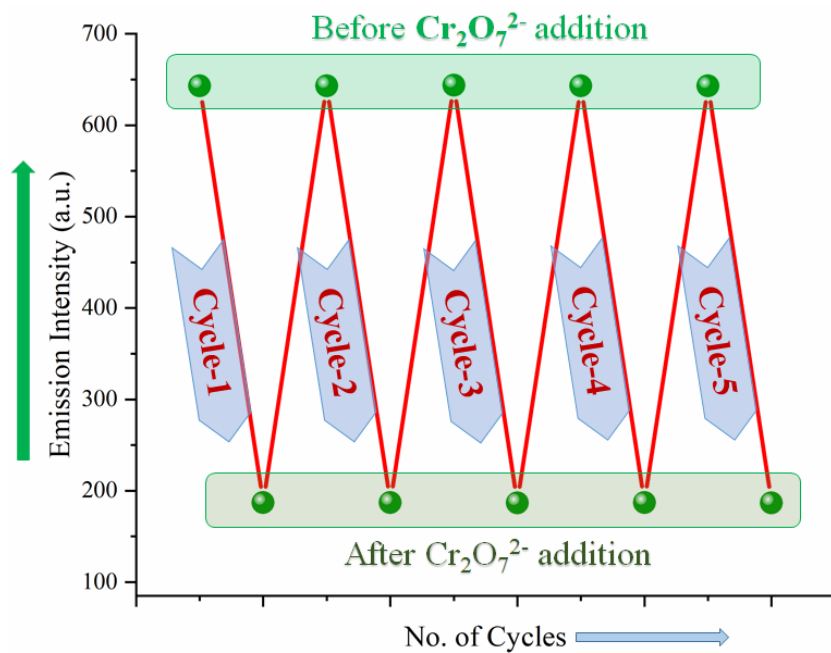**Fig. S49.** Recycling behavior of **1** upto 5 consecutive cycles for one mM solutions of KMnO$_4$.

Fig. S50. Recycling behavior of **1** upto 5 consecutive cycles for one mM solutions of K$_2$Cr$_2$O$_7$.
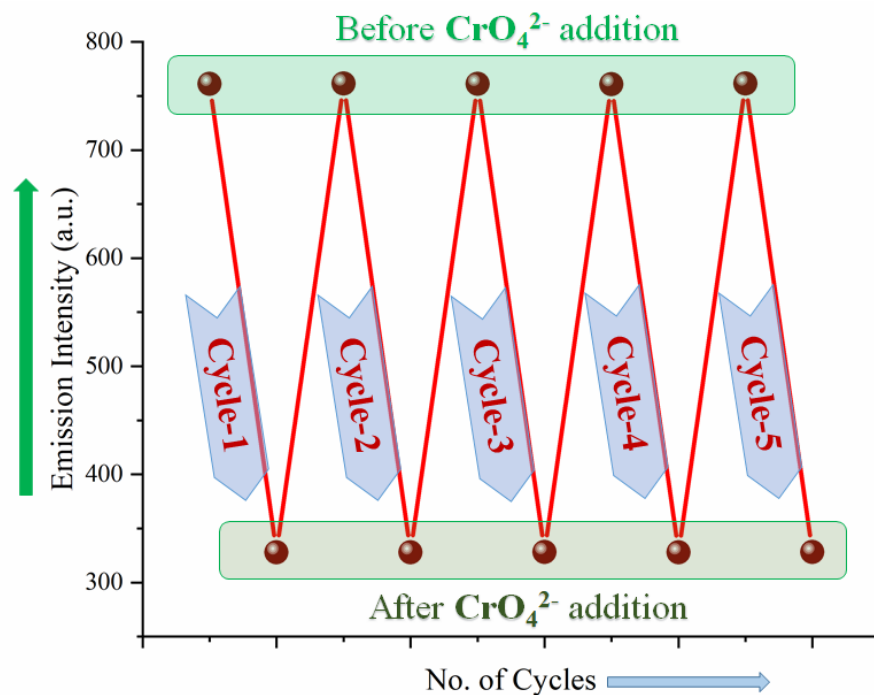
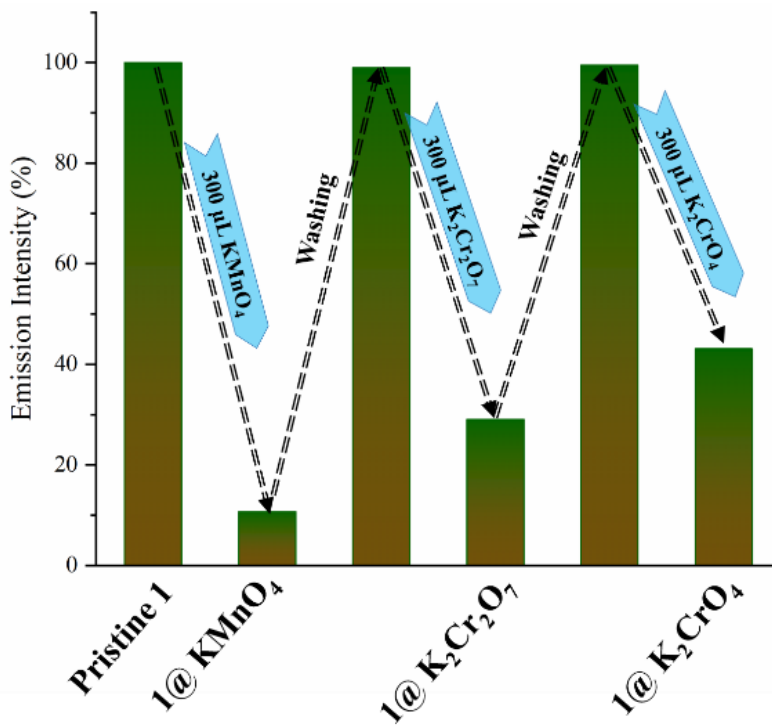**Fig. S51.** Recycling behavior of **1** upto 5 consecutive cycles for one mM solutions of K_2CrO_4.

Fig. S52. Cross sensing experiment: the sensing ability of **1** towards particular oxo-anions and after recovery when **1** is subjected to the sensing of another oxo-anion. The sensing efficiency remain interact in this cross sensing process.
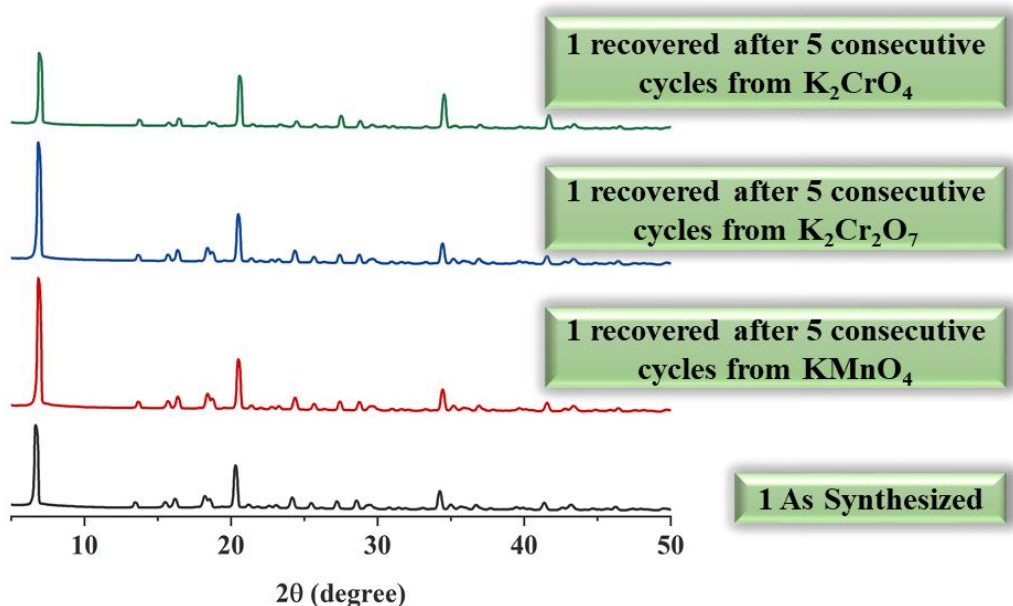
Fig. S53. Powder X-ray patterns of **1** after 5 consecutive sensing cycles for target anions (one mM). The patterns demonstrate that the structure remains intact during the cycles.
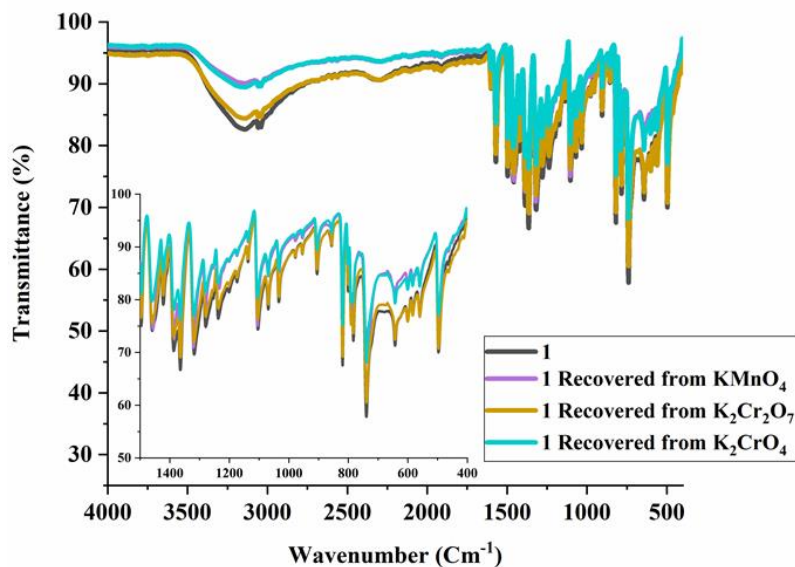

Fig. S54. FT-IR spectrum of as-synthesized **1** and recovered **1** after 5 cycles of sensing study with $KMnO_4$, $K_2Cr_2O_7$ and K_2CrO_4.

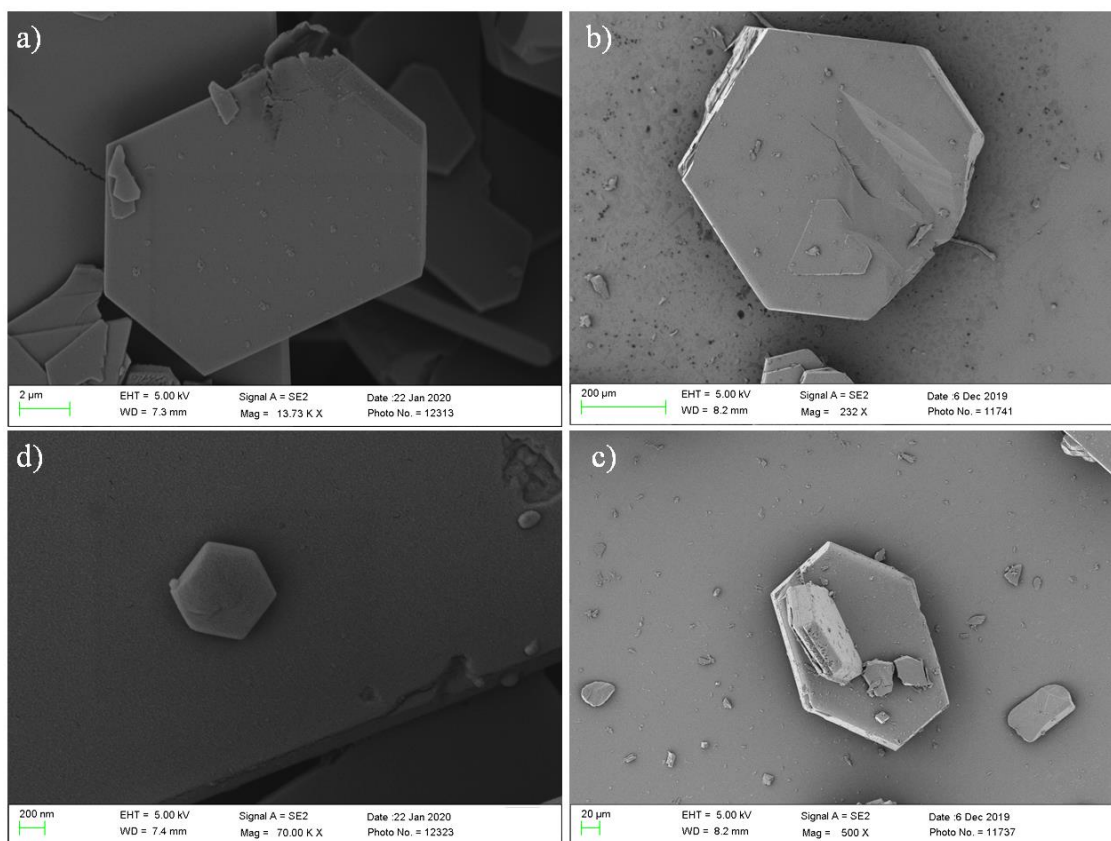**Fig. S55.** Morphological integrity of as-synthesized **1** (a), after sensing of (b) KMnO$_4$, (c) K$_2$Cr$_2$O$_7$ and (d) K$_2$CrO$_4$ respectively.
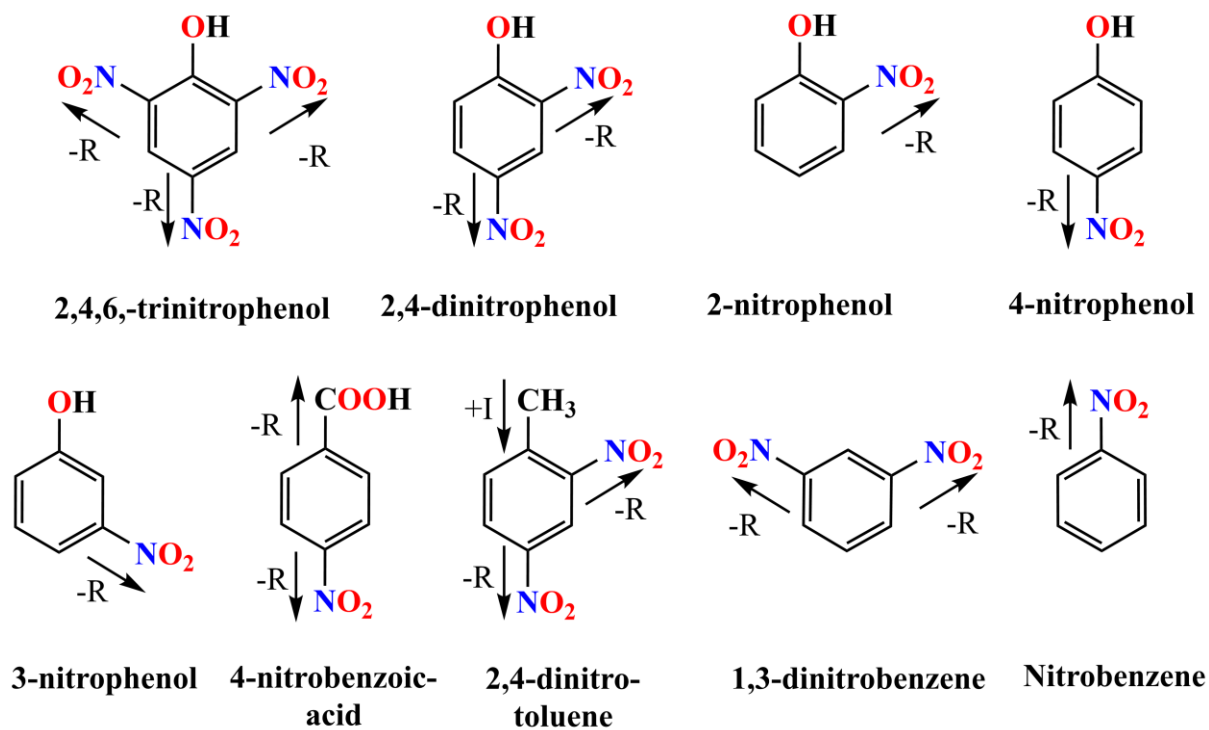
Fig. S56. The various electronic movement in the investigated ONAs that are used in the sensing experiment.
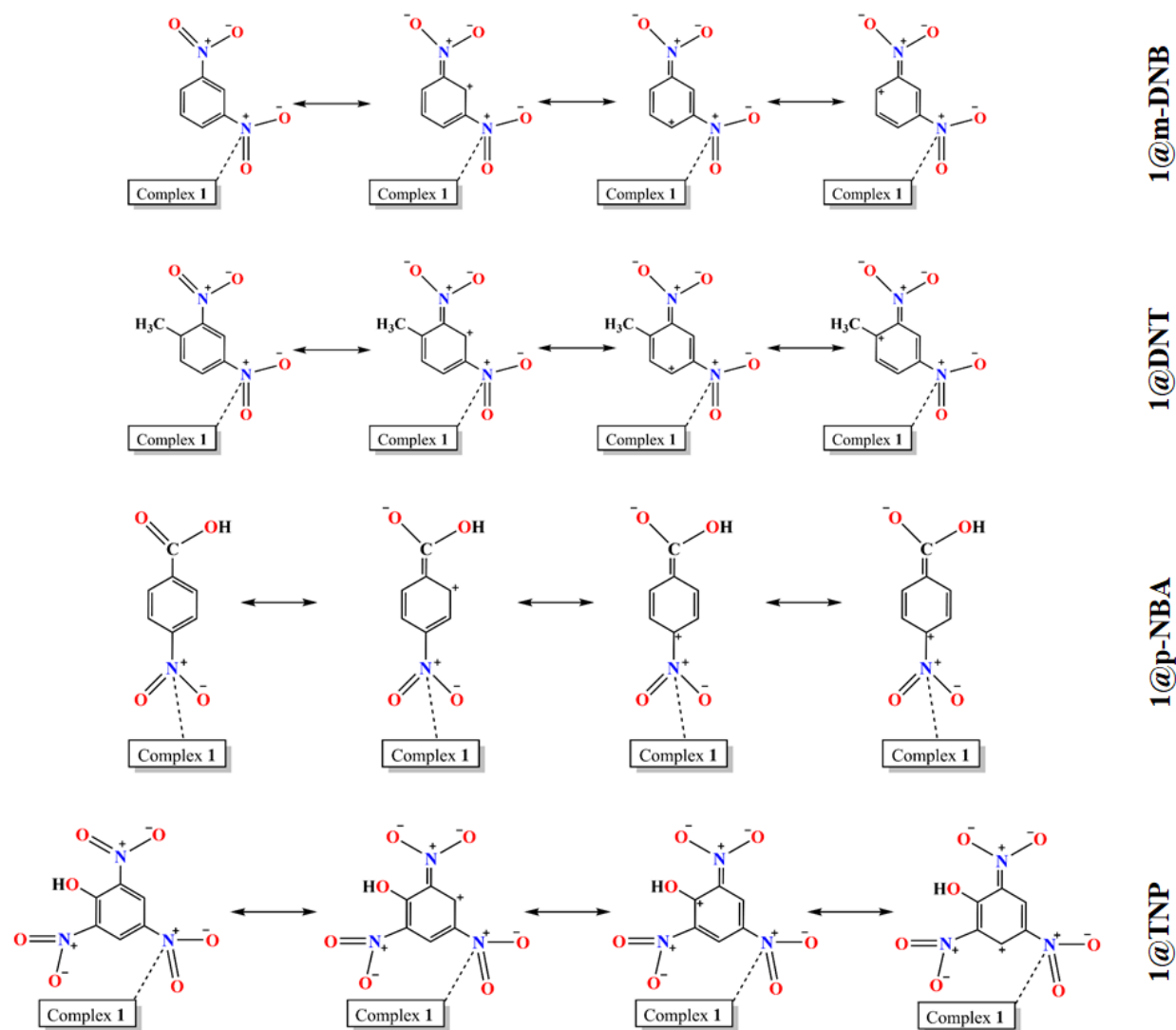
Fig. S57. The various electronic movement in the investigated ONAs that are used in the sensing experiment.

Table S12 Summary of HOMO and LUMO energies of various organic analytes and **1**.

Analytes	HOMO (eV)	LUMO (eV)	Energy gap (eV)
TNP	-8.11	-3.85	4.263
p-NP	-7.16	-2.97	4.19
p-NBA	-7.99	-3.41	4.58
2,4-DNP	-7.68	-3.22	4.46
o-NP	-7.08	-2.93	4.15
m-NP	-7.01	-3.12	3.89

NB	-7.59	-2.82	4.77
2,4-DNT	-8.08	-3.32	4.76
m-DNB	-8.35	-3.44	4.91
1	-4.39	-2.21	2.18
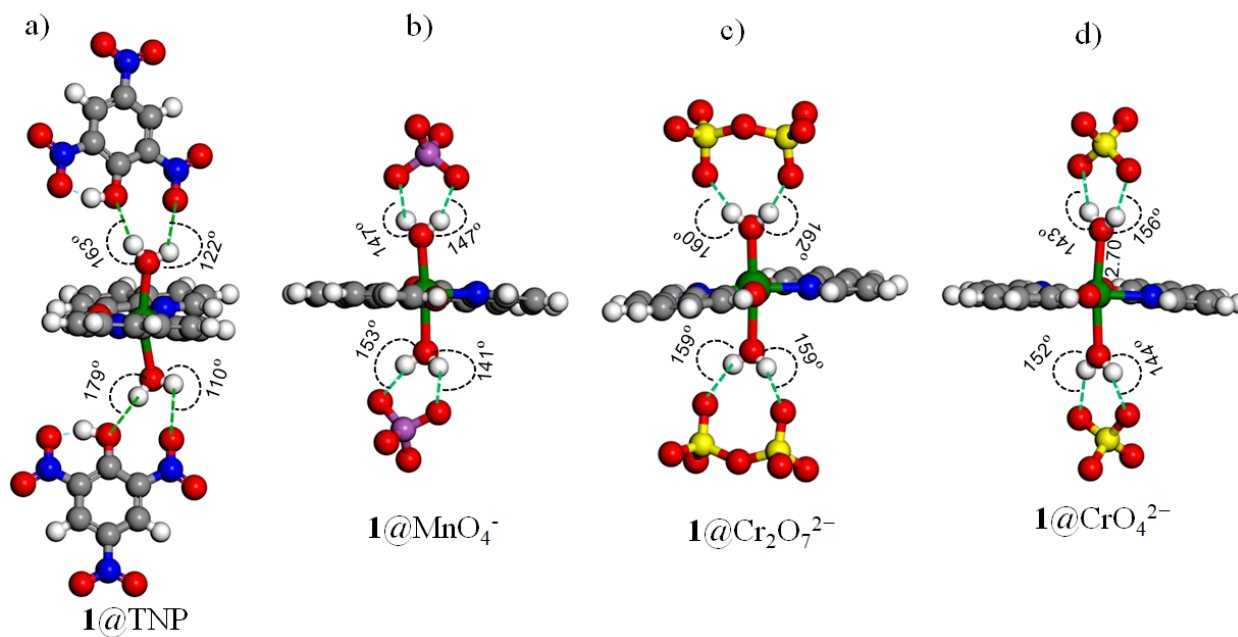
Fig. S58. The bond angles between **1** with the detected lethal analytes: (a) **1**@TNP, (b) **1**@MnO$_4^-$, (c)**1**@Cr$_2$O$_7^{2-}$ and (d) **1**@CrO$_4^{2-}$.

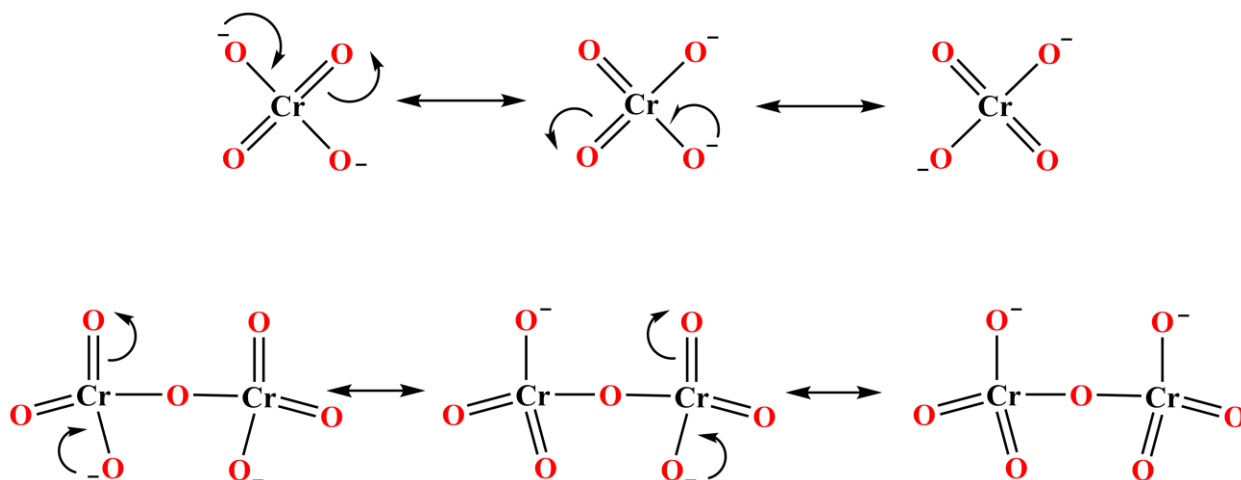**Fig. S59**. The resonance structure of CrO$_4^{2-}$ (above) and Cr$_2$O$_7^{2-}$ (bottom).

Table S13. Summary of HOMO and LUMO energies of various anions derived by performing density functional theory (DFT) in Gaussian 09 package by using B3LYP hybrid function at 6-311++G(d,p) diffused basis set (*Exception for I^- : Hybrid function used is LanL2DZ)

Analytes	HOMO (eV)	LUMO (eV)	Energy gap (eV)
MnO_4^{2-}	-7.75	-3.67	4.08
$Cr_2O_7^{2-}$	-7.27	-2.57	4.70
CrO_4^{2-}	-6.09	-1.08	5.01
SO_4^{2-}	-5.95	0.40	6.35
NO_3^-	-6.49	0.78	7.28
HSO_3^{2-}	-6.47	0.08	6.56
CO_3^{2-}	-4.34	0.52	4.86
I^- *	-5.57	11.61	17.19
Cl^-	-6.74	0.89	7.63
NO_2^-	-5.63	-0.52	5.11
OAc^-	-6.11	0.005	6.12
CN^-	-6.93	-0.88	6.05
$HAsO_4^{2-}$	-5.20	1.47	6.68
AsO_2^-	-4.35	-1.33	3.02
1	-4.39	-2.21	2.18

Table S14. ICP-OES calculations of recovered **1** after sensing of $KMnO_4$, $K_2Cr_2O_7$ and K_2CrO_4.

After 5 consecutive sensing cycles of each analytes, 3 mg of complex **1** was collected for ICP-OES analysis. Collected compound was dissolved in 3 mL of aqua regia solution and the solution was heated at 150 °C until complete dryness. Above process was repeated for 3 times to achieve effective dissolution of anions incorporated with complex **1**. The obtained residue was taken, and the solution was prepared by adding 10 mL of H_2O to it. Freshly prepared solution was further used for ICP-OES study.

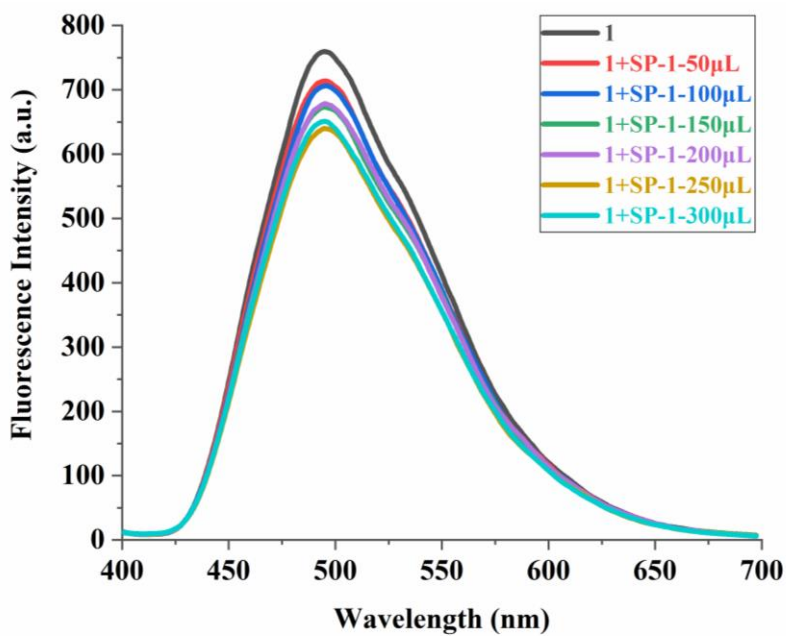| Sample	Amount of Cd^{2+}	Amount of analytes found
1 recovered from $KMnO_4$	222.5 mg/L	0.075 mg/L of Mn^{+7}
1 recovered from $K_2Cr_2O_7$	233.8 mg/L	0.085 mg/L of Cr^{+6}
1 recovered from K_2CrO_4	238.0 mg/L	0.039 mg/L of Cr^{+6}

Fig. S60. The fluorescence titration of **1** upon addition of specimen SP-1 having no targeted analytes.
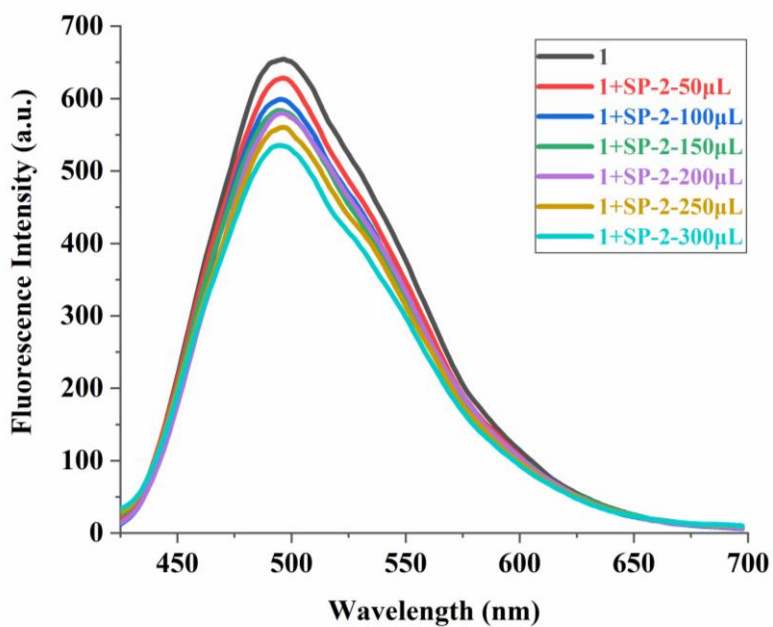

Fig. S61. The fluorescence titration of **1** upon addition of specimen SP-2 having no targeted analytes.
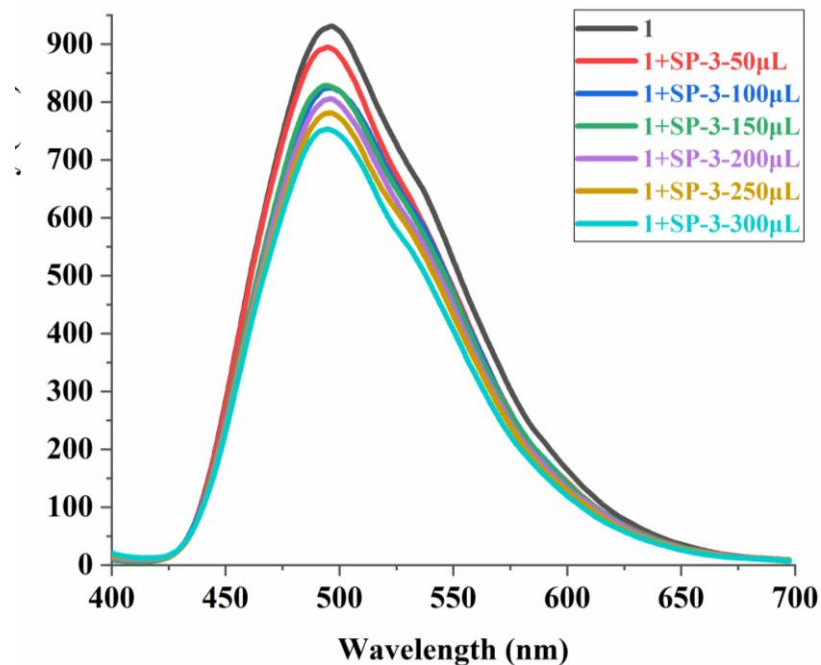.

Fig. S62. The fluorescence titration of **1** upon addition of specimen SP-3 having no targeted analytes.
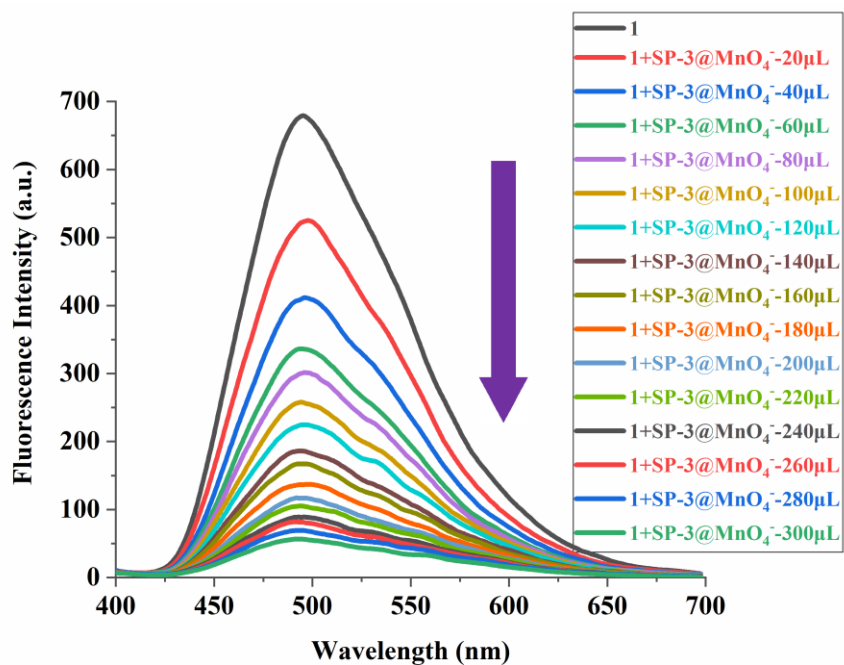

Fig. S63. The fluorescence titration of **1** upon gradual addition of environmental specimens, SP-3 containing MnO_4^- anion of one mM.
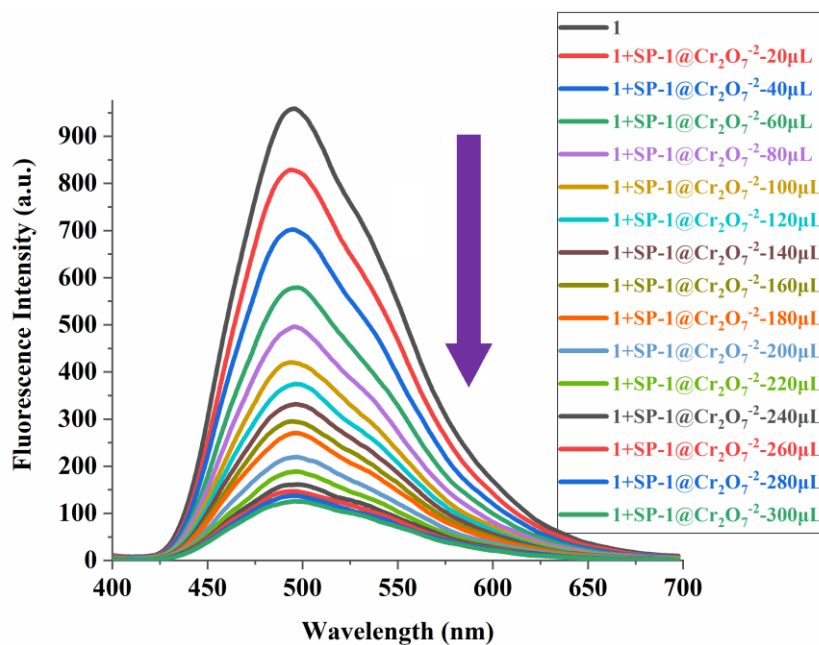
Fig. S64. The fluorescence titration of **1** upon gradual addition of environmental specimens, SP-1 containing $Cr_2O_7^{2-}$ of one mM.

Fig. S65. The fluorescence titration of **1** upon gradual addition of environmental specimens, SP-2 containing $Cr_2O_7^{2-}$ of one mM.

Fig. S66. The fluorescence titration of **1** upon gradual addition of environmental specimens, SP-3 containing $Cr_2O_7^{2-}$ of one mM.

Fig. S67. The fluorescence titration of **1** upon gradual addition of environmental specimens, SP-1 containing CrO_4^{2-} of one mM.
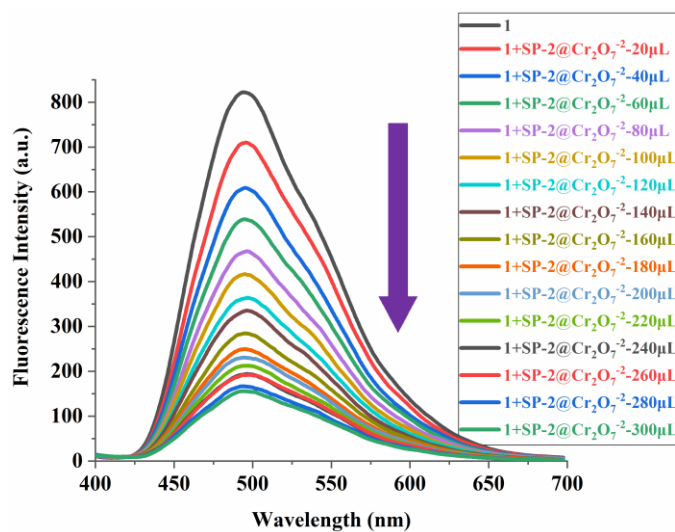
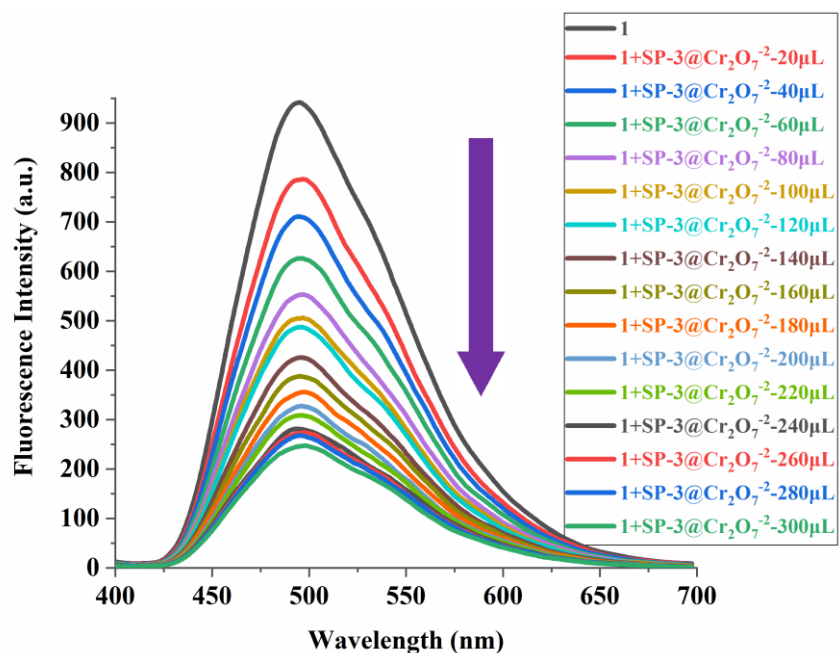**Fig. S68.** The fluorescence titration of **1** upon gradual addition of environmental specimens, SP-2 containing CrO_4^{2-} of one mM.
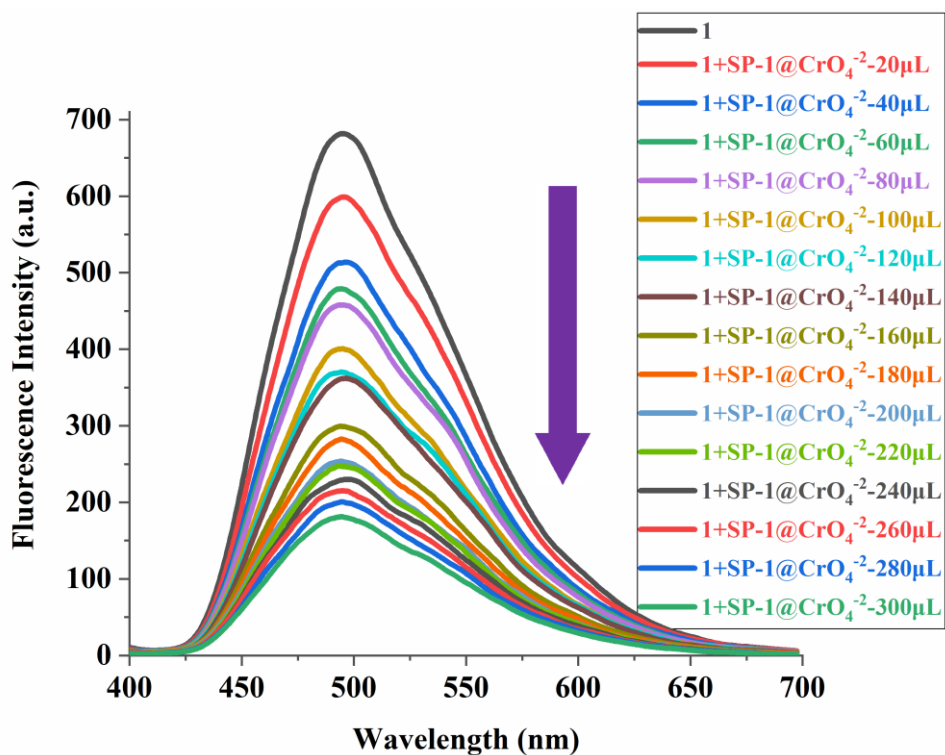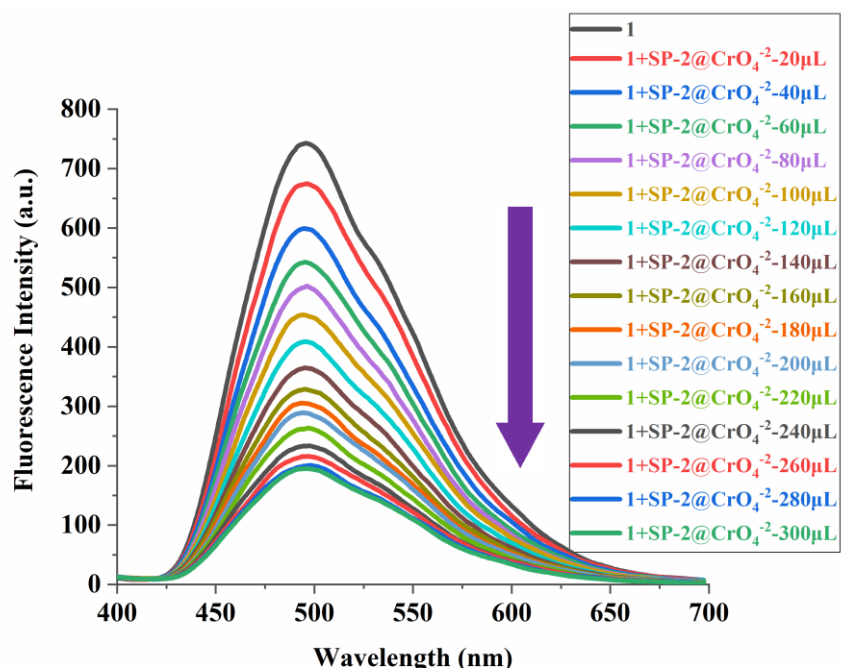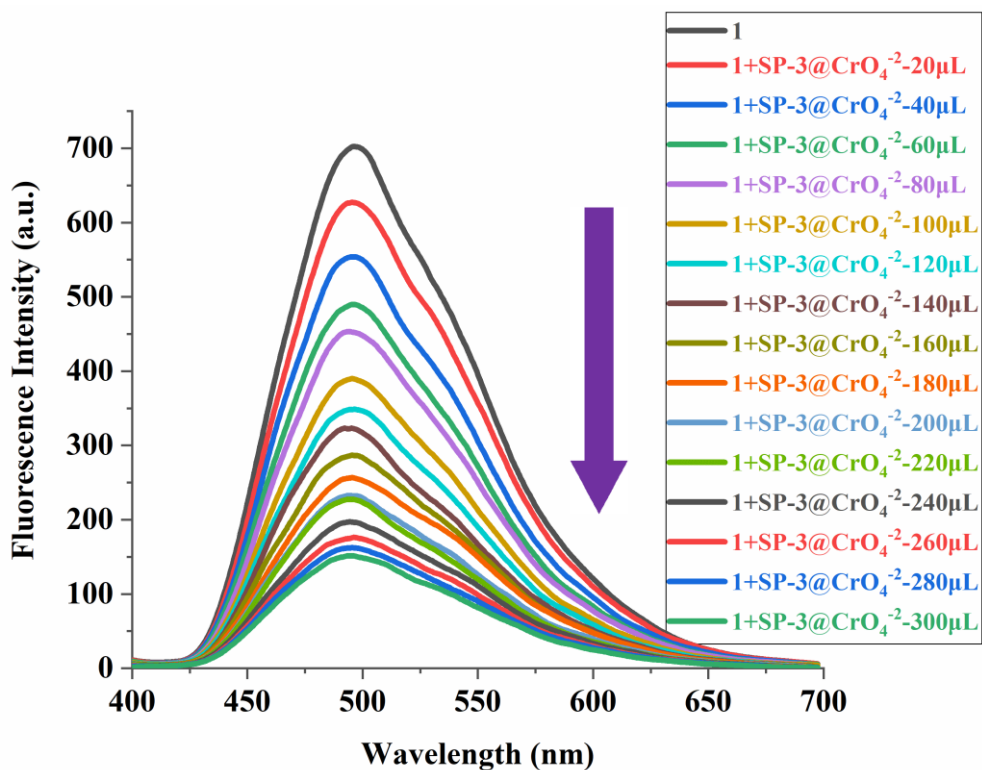

Fig. S69. The fluorescence titration of **1** upon gradual addition of environmental specimens, SP-3 containing CrO_4^{2-} of one mM.

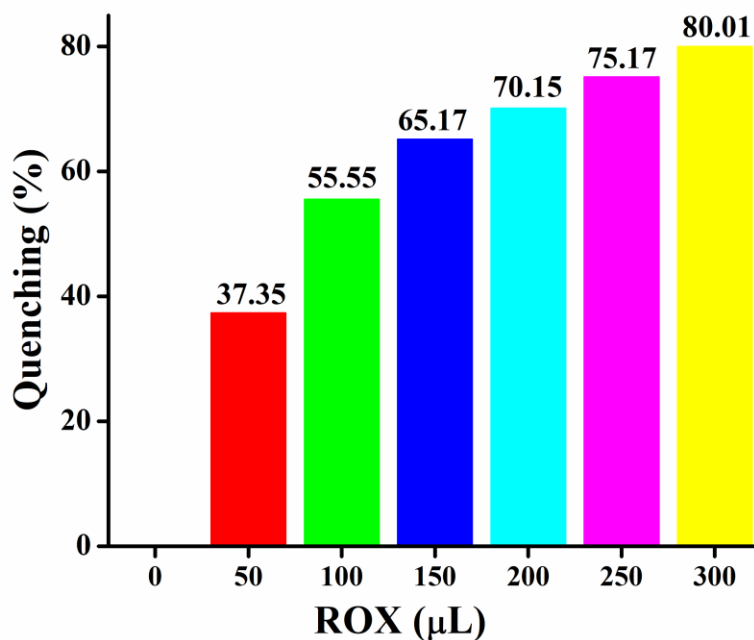**Fig. S70.** The bar diagram represents the quenching efficiency (%) of roxarsone on the luminescent intensity of **1** in dispersed aqueous medium.
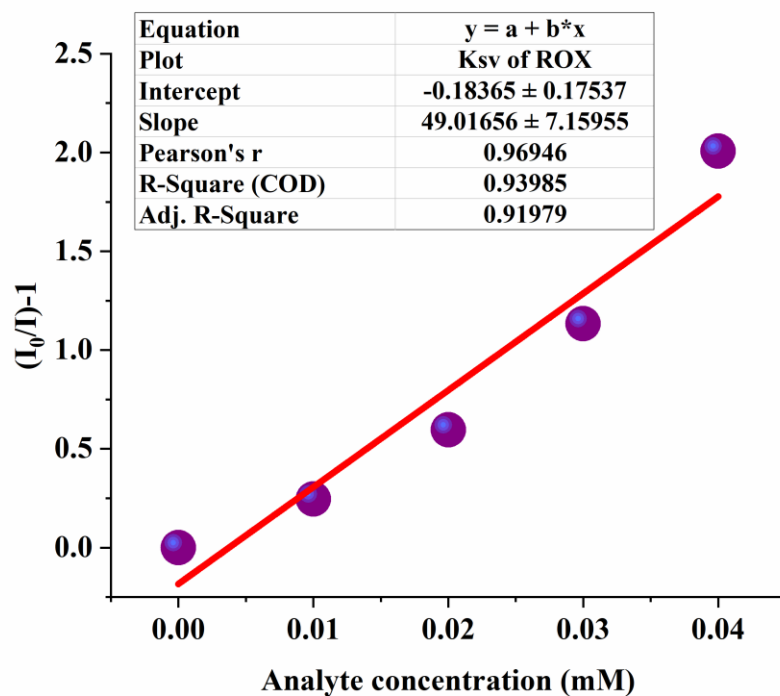

Fig. S71. Stern-Volmer plot for ROX in dispersed aqueous medium of **1**. At lower range, there is a linear relation between the concentration of ROX (0-0.04 mM) with the $[(I_0/I)-1]$ (relative emission intensity) of **1.**
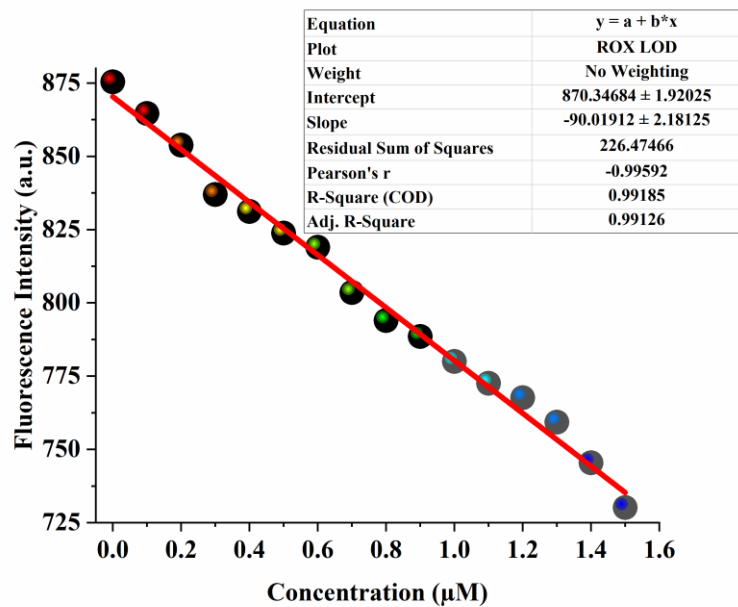
Fig. S72. Linear fitting of fluorescence intensity of **1** upon addition of 10 µM of ROX solution (0 −300 µL).

Table S15. LOD table: standard deviation (Fluorescence intensity) and limit of detection (LOD) calculations for **1** towards ROX.

Blank Readings(1)	Fluorescence Intensity (a.u.)
1	527.41152
2	516.62384
3	526.86504
4	522.77629
5	517.61323
Standard Deviation(σ)	5.034129958
Slope from Plot(M)	90.019 µM^{-1}
Limit of Detection($3\sigma/M$)	0.167 µM/167 nM
Limit of Detection(LOD)	0.073 ppm/73 ppb

References

1 S.Chandra, P. Patra, S. Pathan, S. Roy, S. Mitra, A. Layek, R. Bhar, P. Pramanik and A. Goswami, *J. Mater. Chem. B*, 2013, **1**, 2375-2382.

2 X. Zhai, P. Zhang, C. Liu, T. Bai, W. Li, L. Dai and W. Liu, *Chem. Comm.* 2012, **48***, 7955-7957.

3 International Tables for X-Ray Crystallography, Kynoch Press, Vol. III, Birmingham, England, 1952.

4 *SAINT+*, *version 6.02*; Bruker AXS: Madison, WI, 1999.

5 G. M. Sheldrick, *SADABS*, *Empirical Absorption Correction Program*, University of Gottingen: Gottingen, Germany, 1997.

6 XPREP, 5.1 ed.,Siemens Industrial Automation Inc.: Madison, WI, 1995.

7 G. M. Sheldrick, SHELXTL Reference Manual, version 5.1, Bruker AXS, Madison, WI, 1997.

8 G. M. Sheldrick, SHELXL-2018, Program for Crystal Structure Refinement, University of Gottingen, Gottingen, Germany, 2018.

9 L. J. Barbour, X-Seed 4: Updates to a program for small-molecule supramolecular crystallography. *J. Appl. Cryst.* 2020, **53**, 1141.

10 B. Delley, *J. Chem. Phys.*, 1990, **92**, 508.

11 J. P. Perdew and Y. Wang, *Phys. Rev. B: Condens. Matter Mater. Phys.*, 1992, **45**, 244–248.

12 S. Dhawan, H. Devnani, J. Babu, H. Singh, M. A. Haider, T. S. Khan, P. P. Ingole and V. Haridas, *ACS Appl. Bio Mater.*, 2021, **4**, 2453−2464.

13 T. S. Khan, S. Balyan, S. Mishra, K. K. Pant and M. A. Haider, *J. Phys. Chem. C,* 2018, **122**, 11754−11764.

14 S. Balyan, M. A. Haider, T. S. Khan and K. K. Pant, *Catal. Sci. Technol.*, 2020, **10**, 3857−3867.

15 S. Chandra, P. Patra, S. H. Pathand, S. Roy, S. Mitra, A. Layek, R. Bharb, P. Pramanik and A. Goswami, *J. Mater. Chem. B*, 2013, **1**, 2375-2382.

16 X. Zhai, P. Zhang, C. Liu, T. Bai, W. Li, L. Dai and W. Liu, *Chem. Comm.*, 2012, **48***, 7955-7957.

17 S. Mukherjee, A. V. Desai, A. I. Inamdar, B. Manna and S. K. Ghosh, *Cryst. Growth Des.*, 2015, **15**, 3493-3497.

18 H. Ma, C. He, X. Li, O. Ablikim, S. Zhang and M. Zhang, *Sensors and Actuators B*, 2016, **230**, 746-752.

19 P. Das and S. K. Mandal, *J. Mater. Chem. C*, 2018, **6**, 3288-329.

20 P. G. D. Rosso, M. J. Romagnoli, M. F. Almassio, C. A. Barbero and R. O. Garay, *Sensors and Actuators B*, 2014, **203**, 612-620.

21 Z. –H. Fu, Y. –W. Wang and Y. Peng, *Chem. Commun.*, 2017, **53**, 10524-10527.

22 G. Chakraborty, P. Das and S. K. Mandal. *Mater. Adv.*, 2021, **2**, 2334-2346.

23 Y. Xu, B. Li, W. Li, J. Zhao, S. Sun and Y. Pang, *Chem. Commun.*, 2013, **49**, 4764-4766.

24 Y. Liu, X. Lv, X. Zhang, L. Liu, J. Xie and Z. Chen, *Spectrochimica Acta Part A: Molecular and Biomolecular Spectroscopy*, 2020, **239**, 118497.

25 S. S. Nagarkar, A. V. Desai and S. K. Ghosh, *Chem. Commun.*, 2014, **50**, 8915-8918.

26 J. –D. Xiao, L. –G. Qiu, F. Ke, Y. –P. Yuan, G. –S. Xu, Y. –M. Wang and X. Jiang, *J. Mater. Chem. A*, 2013, **1**, 8745-8752.

27 B. Joarder, A. V. Desai, P. Samanta, S. Mukherjee and S. K. Ghosh, *Chem. Eur. J.*, 2015, 21, 965-969.

28 L. Zhang, J. Hu, J. Li and J. Zhang, *Journal of Luminescence*, 2021, **234**, 117958.

29 D. Majumdar, S. Dey, A. Kumari, T. K. Pal, K. Bankura and D. Mishra, *Spectrochimica Acta Part A: Molecular and Biomolecular Spectroscopy*, 2021, **254**, 119612.

30 B. Wang, X. –L. Lv, D. Feng, L. –H. Xie, J. Zhang, M. Li, Y. Xie, J. –R. Li and H. –C. Zhou, *J. Am. Chem. Soc.*, 2016, **138**, 6204-6216.

31 S. S. Nagarkar, B. Joarder, A. K. Chaudhari, S. Mukherjee and S. K. Ghosh, *Angew. Chem. Int. Ed.*, 2013, **52**, 2881-2885.

32 G. Das, B. P. Biswal, S. Kandambeth, V. Venkatesh, G. Kaur, M. Addicoat, T. Heine, S. Verma, R. Banerjee, *Chem. Sci.*, 2015, **6**, 3931- 3939.

33 S. Dalapati, S. Jin, J. Gao, Y. Xu, A. Nagai and D. Jiang, *J. Am. Chem. Soc.*, 2013, **135**, 17310-17313.

34 G. Lin, H. Ding, D. Yuan, B. Wang and C. A Wang, *J. Am. Chem. Soc.*, 2016, **138**, 3302-3305.

35 P. Das and S. K. Mandal, *J. Mater. Chem. A*, 2018, **6**, 16246-1625.

36 N. Abdollahi and A. Morsali, *Analytica Chimica Acta*, 2019, **1064**, 119-125.

37 Y. Wu, D. Liu, M. Lin and J. Qian, *RSC Adv.*, 2020, **10**, 6022-6029.

38 Y. Cao, Y. Zhang, L. -W. Gu, X. -M. Qin, H. -Y. Li, H. -D. Bian and F. -P. Huang, *New J. Chem.*, 2020, **44**, 10681-10688.

39 Y. –W. Huang, P. –M. Chuang and J. –Y. Wu, *Inorg. Chem.*, 2020, **59**, 9095–9107.

40 B. Li, Q. –Q. Yan and G. –P. Yong, *J. Mater. Chem. C*, 2020, **8**, 11786-11795.

41 Z. –X. Wang, H. –X. Tian, M. Li, M. Zha, B. –L. Li and B. Wu, *Applied Organometallic chemistry*, 2020, **34**, e5977.

42 R. Goswami, N. Seal, S. R. Dash, A. Tyagi and S. Neogi, *ACS Appl. Mater. Interfaces*, 2019, **11**, 40134–40150.

43 M. Li, Z. Cui, S. Pang, L. Meng, D. Ma, Y. Li, Z. Shi and S. Feng, *J. Mater. Chem. C*, 2019, **7**, 11919-11925.